ATLAS Measurements of Rare Decays and CP Violation in Beauty Mesons

Aidan Grummer (University of New Mexico)
On Behalf of the ATLAS Collaboration

SUSY2019
May 20, 2019

Introduction

- Precision measurement of ultra-rare decays $B^0 \to \mu^+\mu^-$ and $B_s^0 \to \mu^+\mu^-$
  - *JHEP 04 (2019) 098*
  - High Luminosity LHC sensitivity projections: **ATL-PHYS-PUB-2018-005**
- CP-violation in the $B_s^0 \to J/\psi\phi$ channel
  - **ATLAS-CONF-2019-009**
  - High Luminosity LHC sensitivity projections: **ATL-PHYS-PUB-2018-041**

$B^0_{(s)} \to \mu^+\mu^-$ Motivation for the Measurement

- The smallness and precision of the predicted branching fractions provides a favorable environment for observing contributions from new physics
- Significant deviations could arise in models involving non-SM heavy particles such as those predicted in
  - Minimal Supersymmetric Standard Model*
  - Minimal Flavor Violation**
  - Two Higgs-Doublet Models †
  - And others‡

"New Physics"

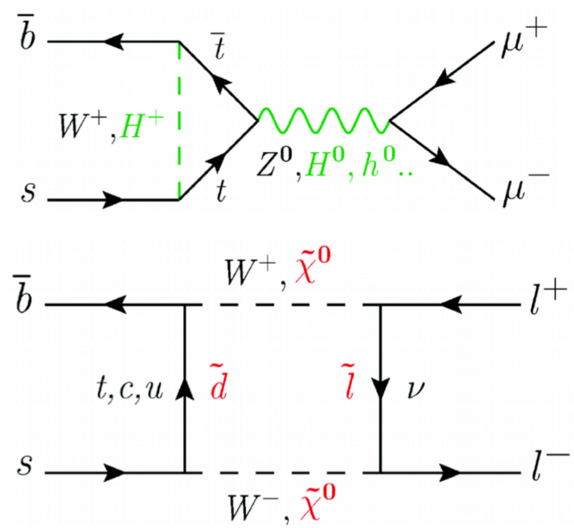

* Huang, Chao-Shang and Liao, Wei and Yan, Qi-Shu, Promising process to distinguish supersymmetric models with large tan β from the standard model: B → X_s μ+ μ−, Phys. Rev. D 59 (1998) 011701, arXiv: hep-ph/9803460 [hep-ph].

** G. D'Ambrosio, G. F. Giudice, G. Isidori and A. Strumia, Minimal flavor violation: an effective field theory approach, Nucl. Phys. B 645 (2002) 155, arXiv: hep-ph/0207036 [hep-ph].

† K. S. Babu and C. F. Kolda, Higgs mediated B^0 → μ+ μ− in minimal supersymmetry, Phys. Rev. Lett. 84 (2000) 228, arXiv: hep-ph/9909476 [hep-ph].

‡ S. Davidson and S. Descotes-Genon, Minimal Flavour Violation for Leptoquarks, JHEP 11 (2010) 073, arXiv: 1009.1998 [hep-ph].

$B^0_{(s)} \to \mu^+\mu^-$ Analysis Background

- The SM precisely predicts* the branching ratios of the two decays:
  - $\mathcal{B}(B^0_s \to \mu^+\mu^-) = (3.65 \pm 0.23) \times 10^{-9}$
  - $\mathcal{B}(B^0 \to \mu^+\mu^-) = (1.06 \pm 0.09) \times 10^{-10}$
- Run 1 results reported by ATLAS** have produced the following branching ratios for the $B^0_{(s)} \to \mu^+\mu^-$ decays
  - $\mathcal{B}(B^0_s \to \mu^+\mu^-) = (0.9^{+1.1}_{-0.8}) \times 10^{-9}$
  - $\mathcal{B}(B^0 \to \mu^+\mu^-) < 4.2 \times 10^{-10}$ at 95% confidence level
- These results are consistent with the Standard Model with a p value of 4.8%, corresponding to 2.0 standard deviations
- LHCb has reported their results from 2015 and 2016 data†:
  - $\mathcal{B}(B^0_s \to \mu^+\mu^-) = (3.0 \pm 0.6^{+0.3}_{-0.2}) \times 10^{-9}$ with 7.8 σ significance
  - $\mathcal{B}(B^0 \to \mu^+\mu^-) < 3.4 \times 10^{-10}$ at 95% confidence level

*C. Bobeth, M. Gorbahn, T. Hermann, M. Misiak, E. Stamou et al., $B_{s,d} \to l^+l^-$ in the Standard Model with Reduced Theoretical Uncertainty, Phys.Rev.Lett. 112 (2014) 101801, arXiv: 1311.0903 [hep-ph].

**ATLAS Collaboration, Study of the rare decays of B^0_s and B^0 into muon pairs from data collected during the LHC Run 1 with the ATLAS detector, Eur. Phys. J. C76 (2016) 513, arXiv: 1604.04263 [hep-ex].

† LHCb Collaboration, Measurement of the $B^0_s \to \mu^+\mu^-$ Branching Fraction and Effective Lifetime and Search for $B^0 \to \mu^+\mu^-$ Decays, Phys. Rev. Lett. 118 191801, 2017, https://link.aps.org/doi/10.1103/PhysRevLett.118.191801.

Performing the Measurement

- The aim of the measurement is to obtain the branching fraction of the $B^0_{(s)} \to \mu^+\mu^-$ channels
- The branching ratios are made relative to the normalization decay $B^+ \to J/\psi K^+$ which is abundant and has a well measured branching fraction

$$\mathcal{B}(B^0_{(s)} \to \mu^+\mu^-) = \frac{N_{d(s)}}{\varepsilon_{\mu^+\mu^-}} \times [\mathcal{B}(B^+ \to J/\psi K^+) \times \mathcal{B}(J/\psi \to \mu^+\mu^-)] \frac{\varepsilon_{J/\psi K^+}}{N_{J/\psi K^+}} \times \frac{f_u}{f_{d(s)}}$$

- Here $N_{d(s)}$ is the signal yield, $N_{J/\psi K^+}$ is the reference yield, $\varepsilon_{d(s)}$ and $\varepsilon_{J/\psi K^+}$ are the acceptance times the efficiency and $f_u/f_{d(s)}$ is the ratio of the hadronization probabilities of a b-quark into $B^+$and $B^0_{(s)}$.

Preliminary Steps of the Analysis

- Collect the data with the ATLAS detector for analysis
  - Inner Detector
  - Muon Spectrometer

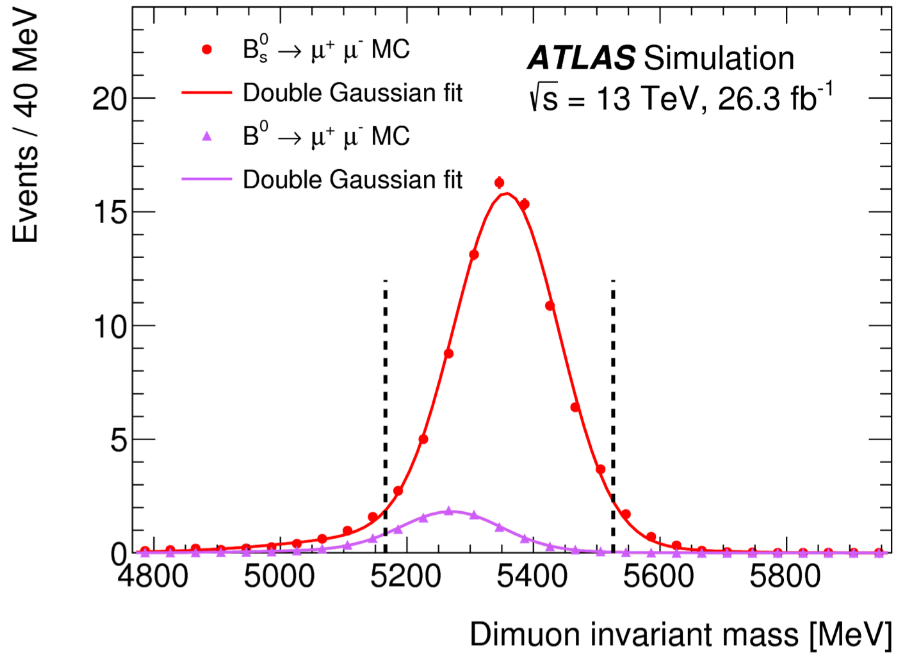

- Perform a **blind analysis**
  - The signal region of the dimuon invariant mass (5166 to 5526 MeV) is concealed while procedures of the event selection and details of the signal extraction are defined
- Simulate the data
  - Dimuon events – for signal and background regions
  - $B^+ \to J/\psi K^+$candidates (reference channel)

Sources of Background

- Continuum background: the dominant combinatorial component
  - Consists of muons from uncorrelated hadron decays
  - Characterized by a weak dependence on the dimuon invariant mass
- Partially reconstructed decays: one or more of the final-state particles (X) in a b hadron decay is not reconstructed
  - These candidates accumulate in the low dimuon invariant mass sideband
- Peaking background: $B^0_{(s)} \rightarrow hh'$ decays with both hadrons misidentified as muons

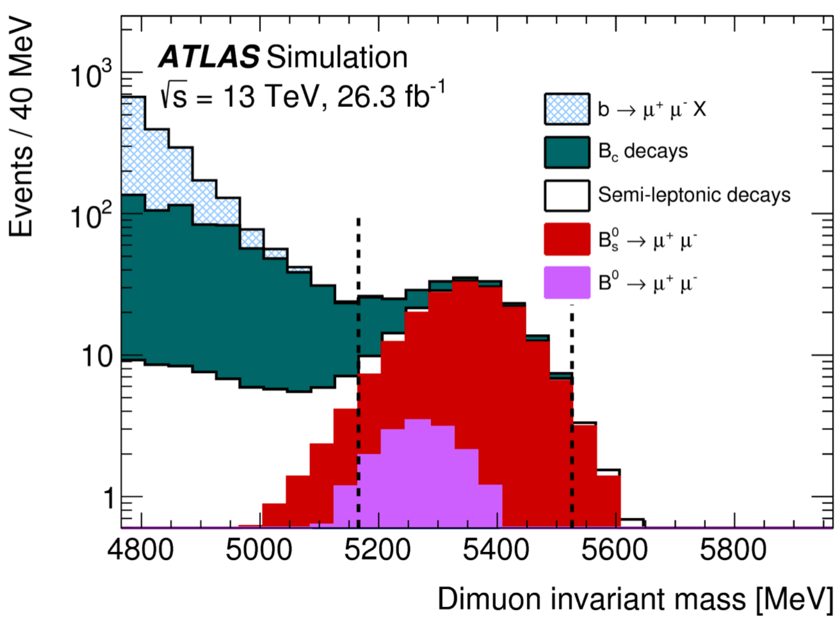

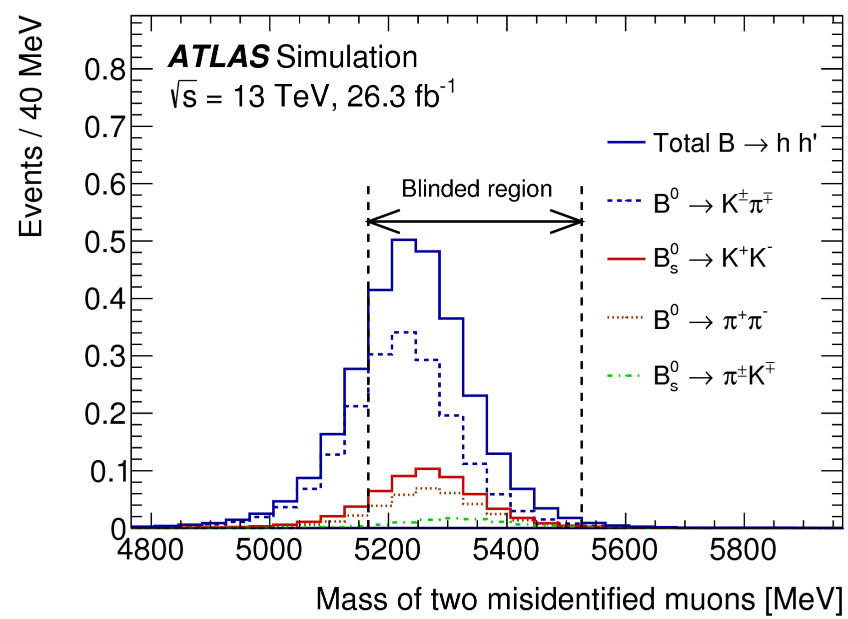

Suppressing the Continuum Background: Multivariate Analysis

- A multivariate approach, implemented as a Boosted Decision Tree (BDT), is used to enhance the signal relative to the continuum background

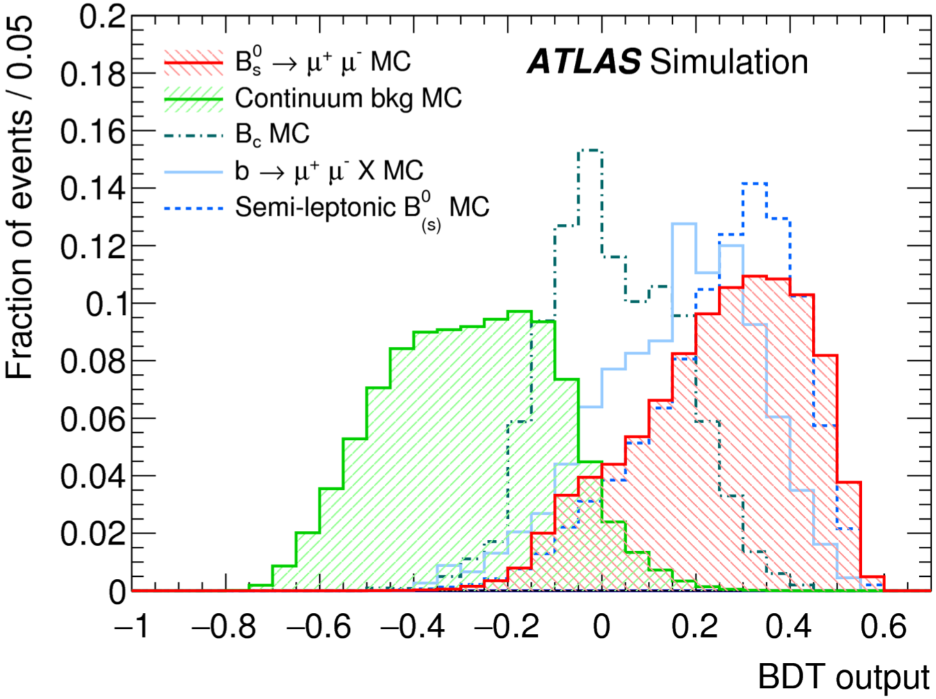

- Here is the final BDT output for various datasets used in the analysis
- A larger BDT output corresponds to more suppression of the continuum background

Data-Simulation Comparisons

- The BDT is optimized when trained with 15 selected input variables - used to characterize a B meson event and the produced muons
- A grid search is performed to optimize the other BDT parameters

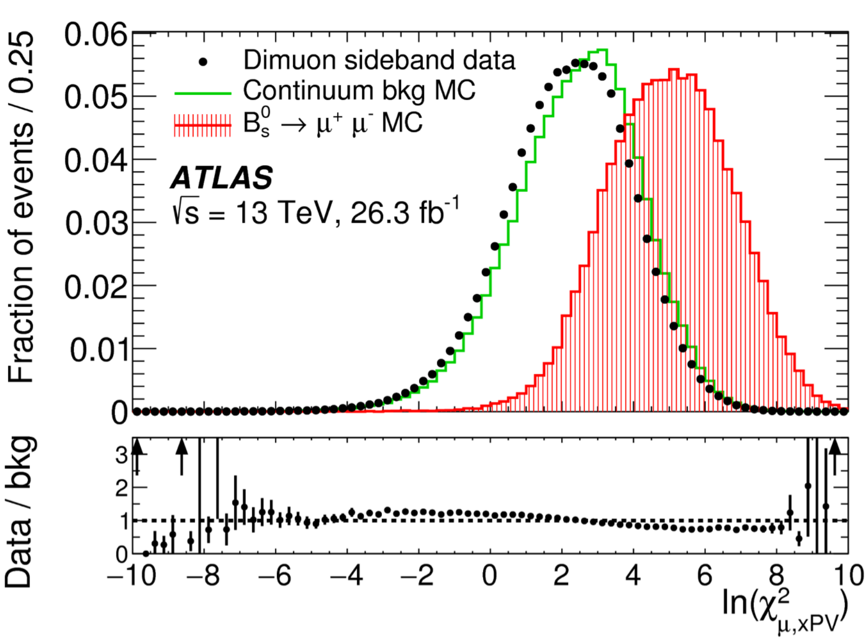

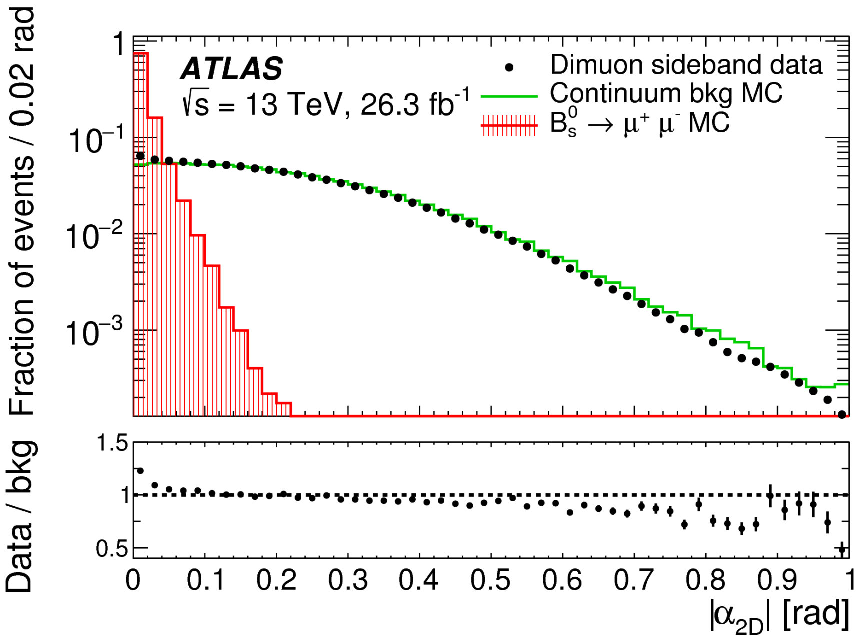

- Shown here are two of the input variables used in the training
- Care is taken to ensure that BDT output is not correlated with the invariant mass of the muons

Yield Extraction
The Normalization Channel

- The $B^{\pm}$ yield for the normalization channel is extracted with an unbinned extended maximum-likelihood fit to the $J/\psi K^{+}$ invariant mass distribution

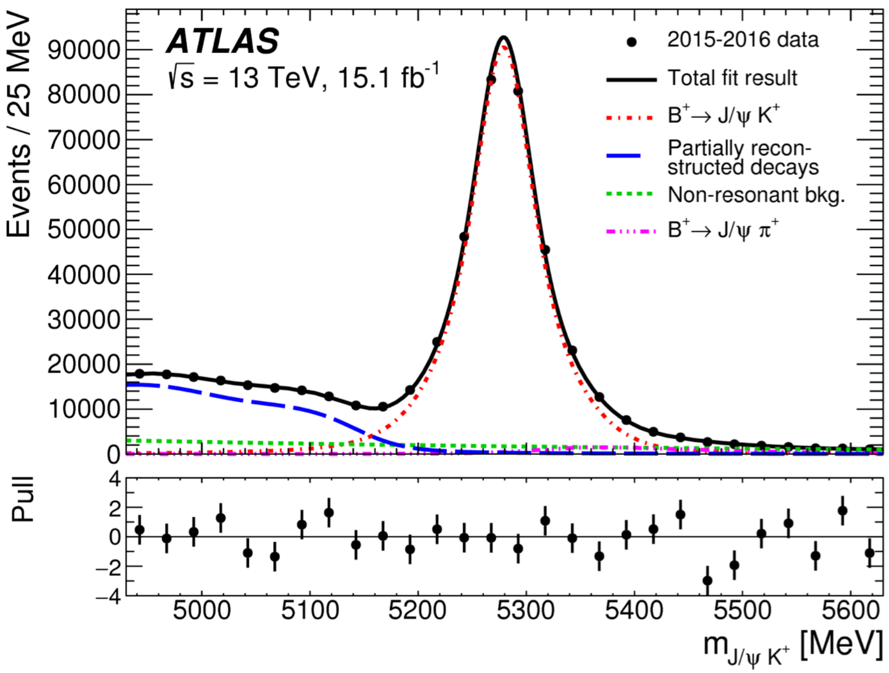

- The fit includes 4 components
  - $B^{+} \rightarrow J/\psi K^{+}$ decays
  - Cabibbo-suppressed $B^{+} \rightarrow J/\psi\pi^{+}$ decays
  - Partially reconstructed B decays
  - Continuum background (composed mostly of $b\bar{b} \rightarrow J/\psi X$ decays)

Efficiency Ratio

- The efficiency ratio is required for the calculation of the signal branching fraction:

$$R_\varepsilon = \frac{\varepsilon\left(B^+ \to J/\psi\, K^+\right)}{\varepsilon\left(B^0{}_{(s)} \to \mu^+\mu^-\right)}$$

- Both channels are measured in the fiducial acceptance for the B meson:
  - $p_T^B > 8$ GeV and $|\eta_B| < 2.5$
- The total efficiencies include acceptance and trigger, reconstruction and selection efficiencies.
  - Muon acceptance: $p_T^{\mu_1} > 6.0$ GeV, $p_T^{\mu_2} > 4.0$ GeV and $|\eta_{\mu_{1,2}}| < 2.5$
  - Kaon acceptance: $p_T^K > 1.0$ GeV and $|\eta_K| < 2.5$
  - The signal reference BDT selection: BDT > 0.2455

Extraction of the Signal Yield

- The data in the dimuon signal region is **unblinded**
- The dimuon candidates are classified according to **four intervals** in the BDT output
- Each interval is chosen to give an equal efficiency of 18% for signal MC events

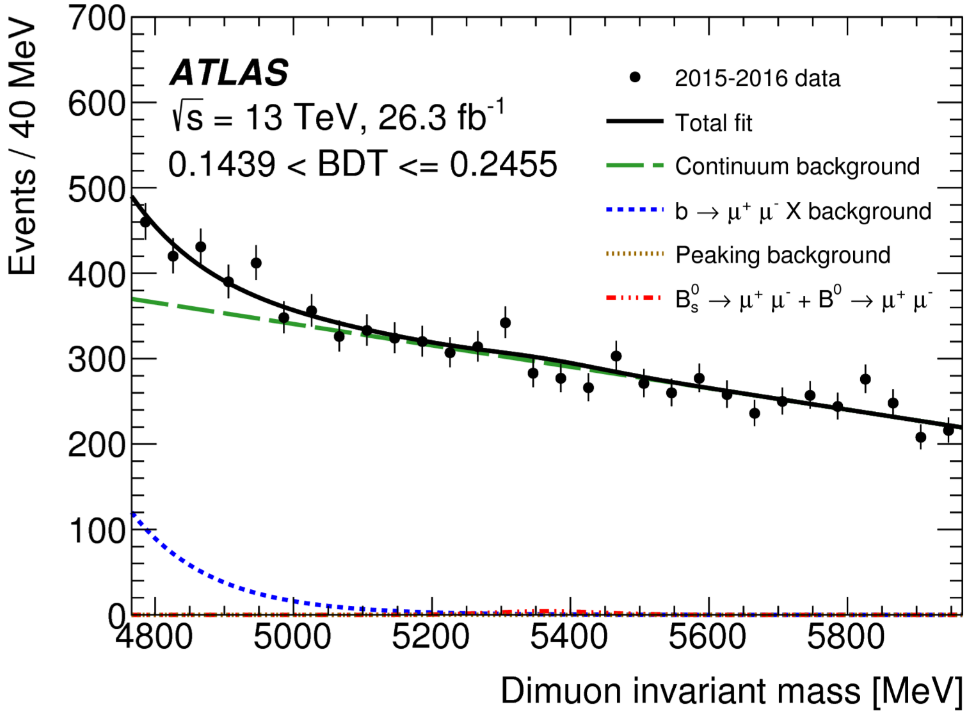

- The figure here shows the BDT interval with the lowest signal to background ratio
- Continuum and partially reconstructed B decays are the main backgrounds

Signal Yield

- Increasing the restrictions of the BDT improve suppression of the continuum background
- Superimposed on each figure is the maximum likelihood fit
- SM Expected:

  $N_s = 91$ and $N_d = 10$
- Determined from the fit of highest bin:

  $N_s = 80 \pm 22$ and $N_d = -12 \pm 20$

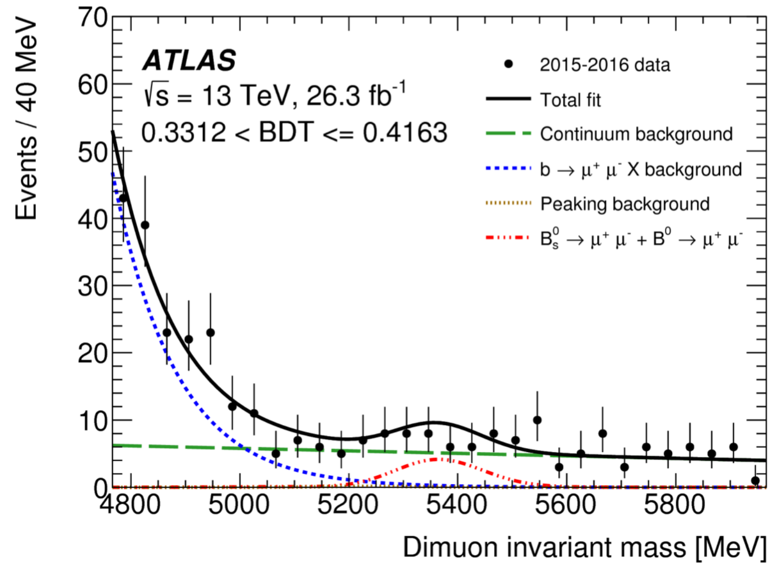

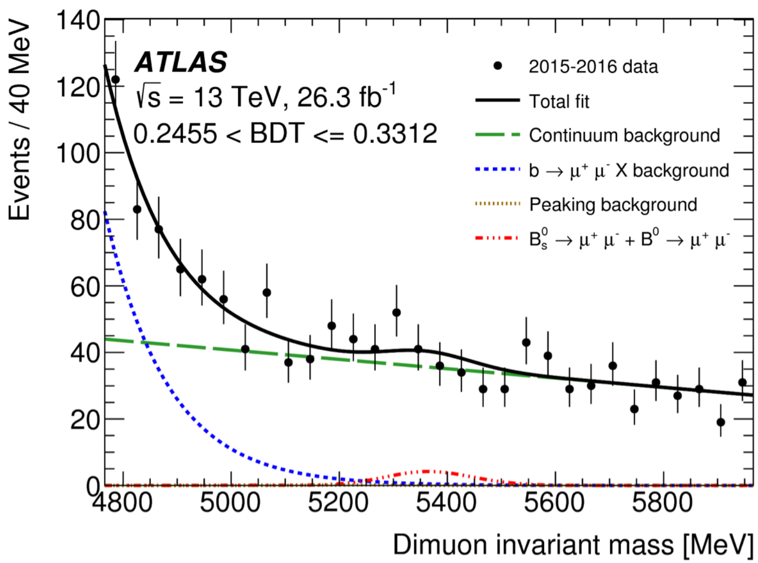

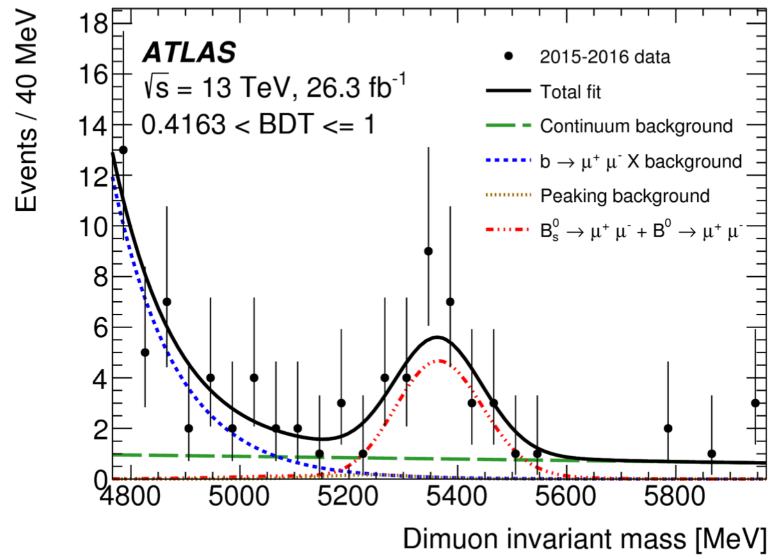

Comparison to the Standard Model

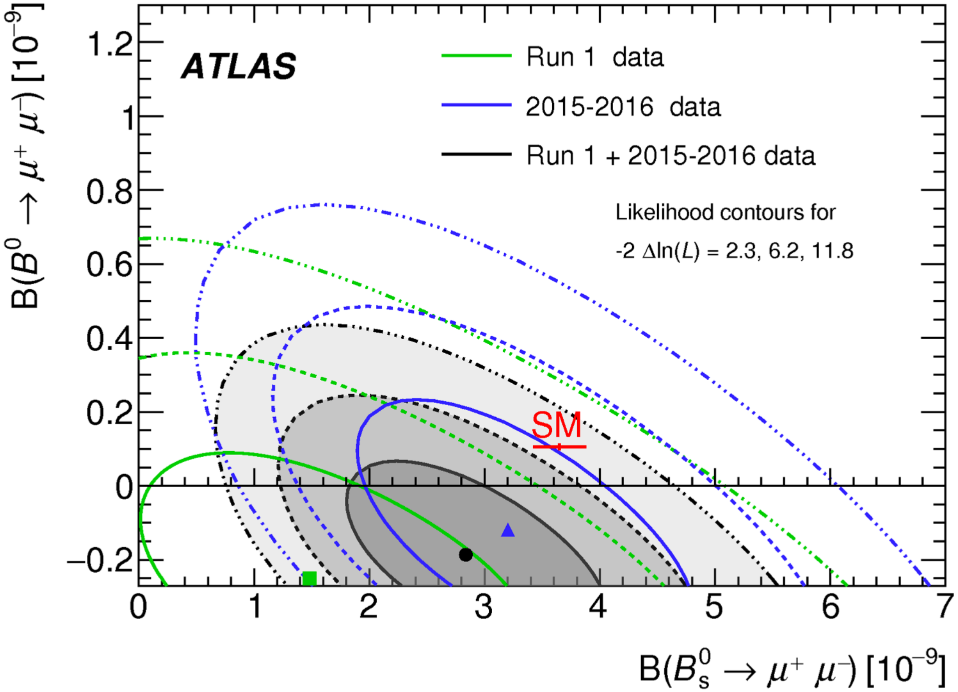

- Simultaneous maximum likelihood fits of the branching ratios of the B^0 and B_s^0.
  - The blue point and contours is the result from 2015 and 2016 data,
  - the green point and contours is the Run 1 result,
  - and the black point and contours is the combination of the two
- Also shown is the Standard Model prediction; the data and the model differ by 2.4 standard deviations
- The significance of $B_s^0 \to \mu^+\mu^-$ combined result is estimated to be 4.6σ

Comparison to the LHCb Result

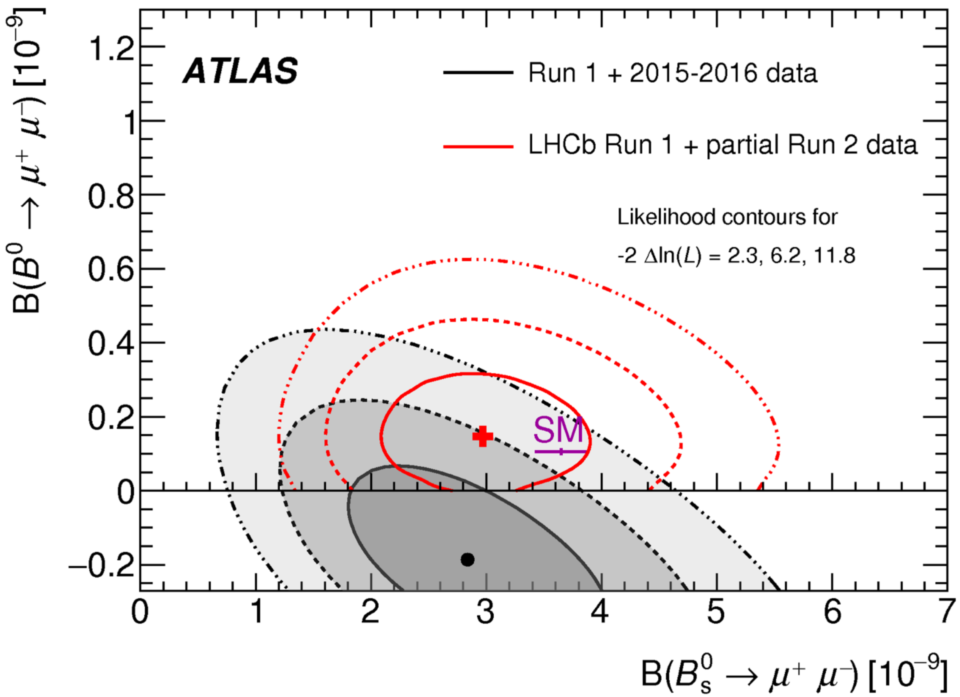

- Comparison of the branching ratios of the B^0 and B_s^0 for the latest ATLAS and LHCb results
  - The black point and contours are the ATLAS combined Run 1 and 2015 and 2016 data result
  - The red point and contours are the LHCb combined Run 1 and partial Run 2 data result
- Also shown is the Standard Model prediction in purple

$B^0_{(s)} \to \mu^+\mu^-$ Projections

- Full Run 2 projections are shown on the right
- HL-LHC projected results shown below

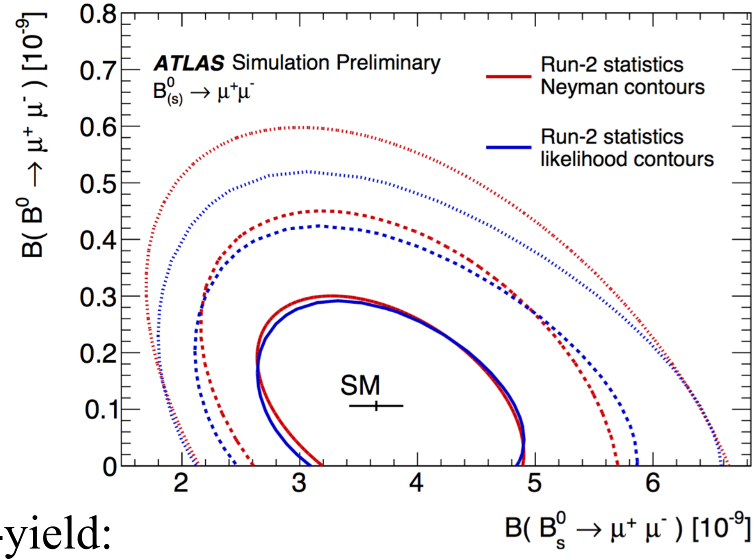

Conservative yield:

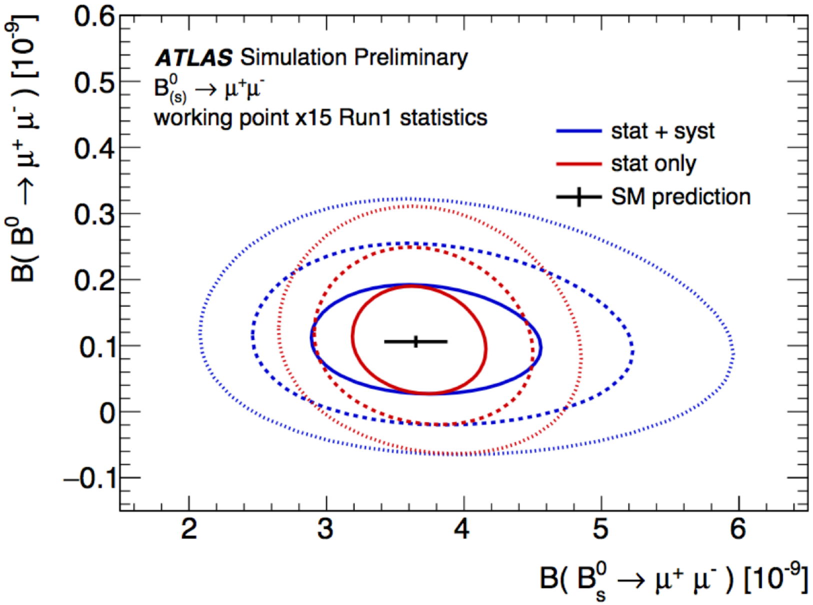

High-yield:

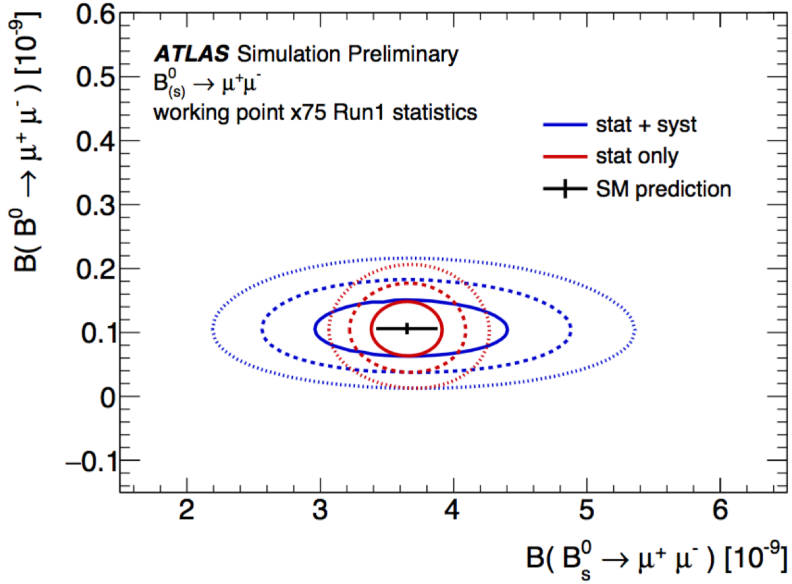

ATLAS Collaboration, ATL-PHYS-PUB-2018-005

CP Violation in $B_s^0 \to \mathrm{J}/\psi\phi$

CP Violation in $B_s^0 \rightarrow J/\psi\phi$

- In the $B_s^0 \rightarrow J/\psi\phi$ decay, CP violation occurs due to interference between a direct decay and a decay with $B_s^0 - \bar{B}_s^0$ mixing

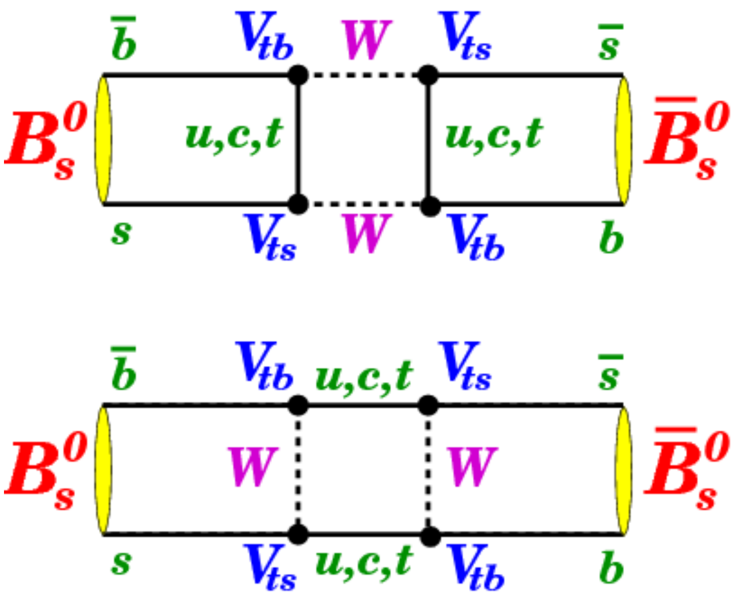

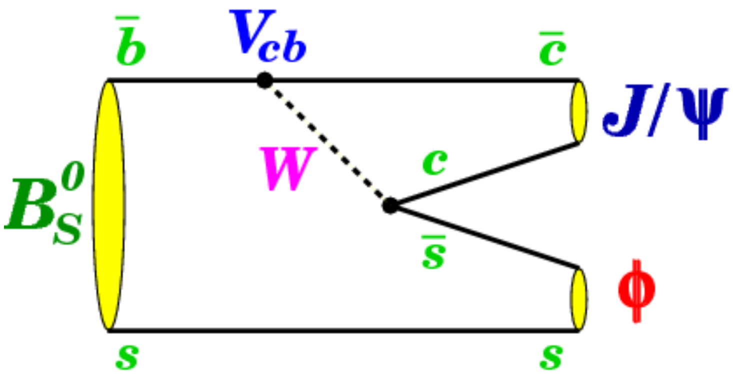

- Shown on the left are the lowest order mixing diagrams that show the mixing oscillations
- On the right is the decay channel of interest

FERMILAB-PUB-11-646-E

CP Violation Parameters

- The CP violating phase ϕ_s is defined as the weak phase difference between the $B_s^0 - \bar{B}_s^0$ mixing amplitude and the $b \rightarrow c\bar{c}s$ decay amplitude
- In the SM the phase ϕ_s is small and is related to Cabibbo–Kobayashi–Maskawa (CKM) quark mixing matrix elements via the relation $\phi_s \approx -2\beta_s$
- In terms of the CKM quark mixing matrix elements, $\beta_s = \arg(-\frac{V_{ts}V_{tb}^*}{V_{cs}V_{cb}^*})$
- In the Standard Model (without New Physics contributions): $-2\beta_s = -0.0363^{+0.0016}_{-0.0015}$
- Other physical quantities involved in the $B_s^0 - \bar{B}_s^0$ mixing are
  - The decay width: $\Gamma_s = (\Gamma_\mathrm{L}+\Gamma_\mathrm{H})/2$
  - And the width difference: $\Delta\Gamma_s = \Gamma_\mathrm{L} - \Gamma_\mathrm{H}$
  - Here, Γ_L and Γ_H are the decay widths of the light and heavy mass eigenstates

Recap of the ATLAS LHC Run 1 Results

- In LHC Run 1 ATLAS experimentally determined ϕ_s and $\Delta\Gamma_s$ to be
  - ϕ_s = -0.090 ± 0.078 (stat.) ± 0.041 (syst.) rad
  - $\Delta\Gamma_s$ = 0.085 ± 0.011 (stat.) ± 0.007 (syst.) ps^{-1}
- These results are compatible with the Standard Model and with other experiments
- The results also leave room for new physics contributions to the CP Violation phase

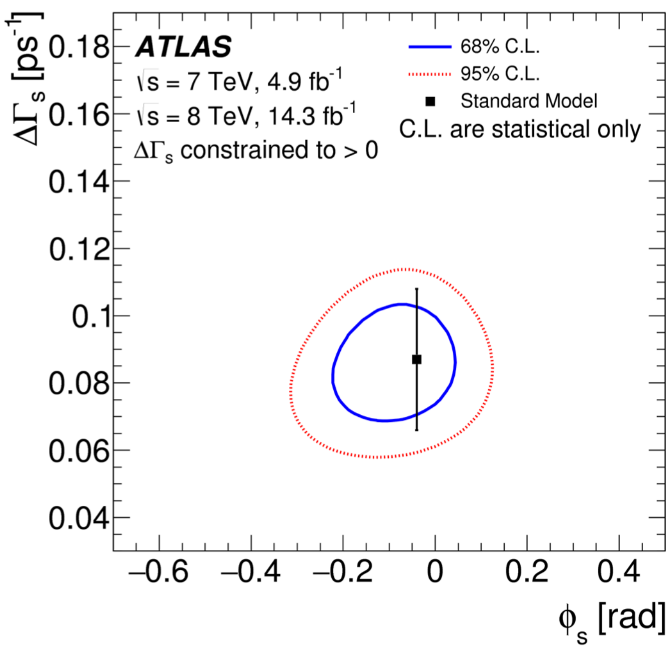

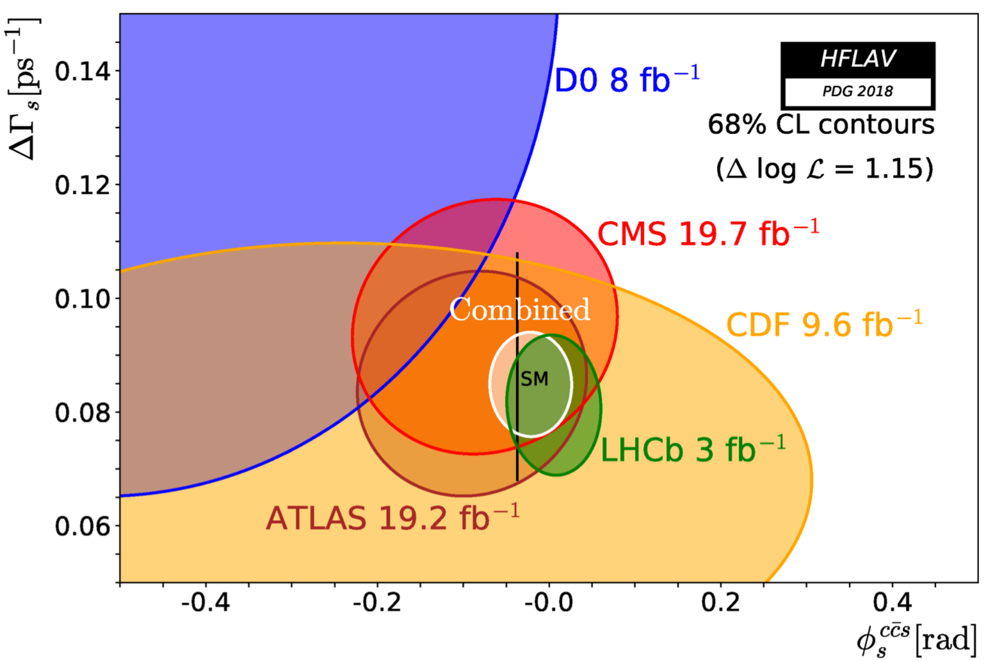

Run 2 Analysis Strategy

- Select events with the use of flavor tagging to identify the flavor of the signal B Meson
- Determine B_s^0 properties:
  - Mass (m_i), mass error (σ_{m_i}), proper decay time (t_i), decay time error (σ_{t_i}), transverse momentum (p_{T_i}), and the tag probability of a B meson flavor: $P_i(\, B|Q_x\,)$
- Determine transversity angles:
  - θ_T, ϕ_T, and ψ_T

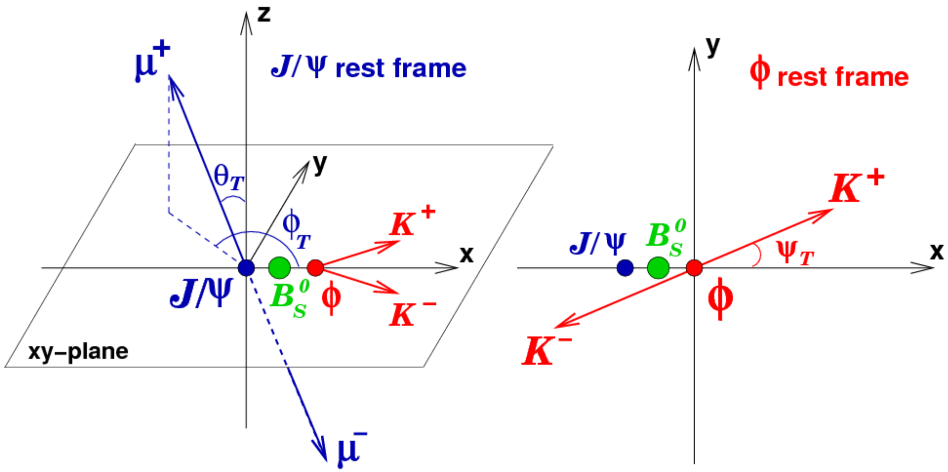

- Perform an unbinned maximum likelihood fit to extract nine parameters simultaneously:
  - The CPV phase and decay widths: ϕ_s, $\Delta\Gamma_s$, Γ_s
  - The amplitudes and strong phases: $|A_0(0)|^2$, $|A_\parallel(0)|^2$, $\delta_\parallel$, $\delta_\perp$, $|A_s(0)|^2$, $\delta_\perp - \delta_s$

Run 2: B_s^0 Flavor Tagging (I)

- The measured charge of a lepton (electron or muon) from the semileptonic decay of a B meson provides strong discrimination for determining the B_s^0 flavor
- Input for B_s^0 flavor tagging:
  - Electron tagging
  - Muon tagging
  - *b*-hadron jet tagging (in the case of no lepton)

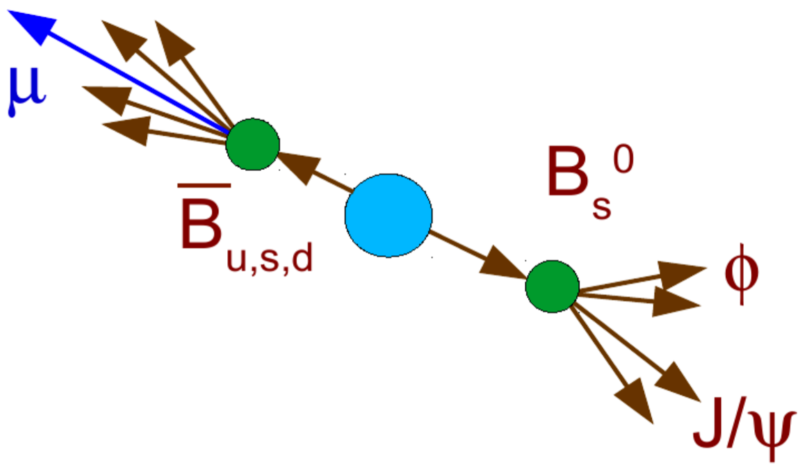

Run 2: B_s^0 Flavor Tagging (II)

- $b \to l$ transitions are diluted through processes that can change the charge of the observed lepton, such as through neutral B meson oscillations, or through cascade decays $b \to c \to l$
- The separation power of lepton tagging is enhanced by considering p_T weighted charge of the tracks in a cone around the electron or muon or charged tracks in the *b*-jet:

$$Q_x = \frac{\sum_i^{N \text{ tracks}} q_i \cdot (p_{\mathrm{T}i})^\kappa}{\sum_i^{N \text{ tracks}} (p_{\mathrm{T}i})^\kappa}$$

- $B^\pm \to \mathrm{J}/\psi K^\pm$ is used to calibrate the flavor tagging

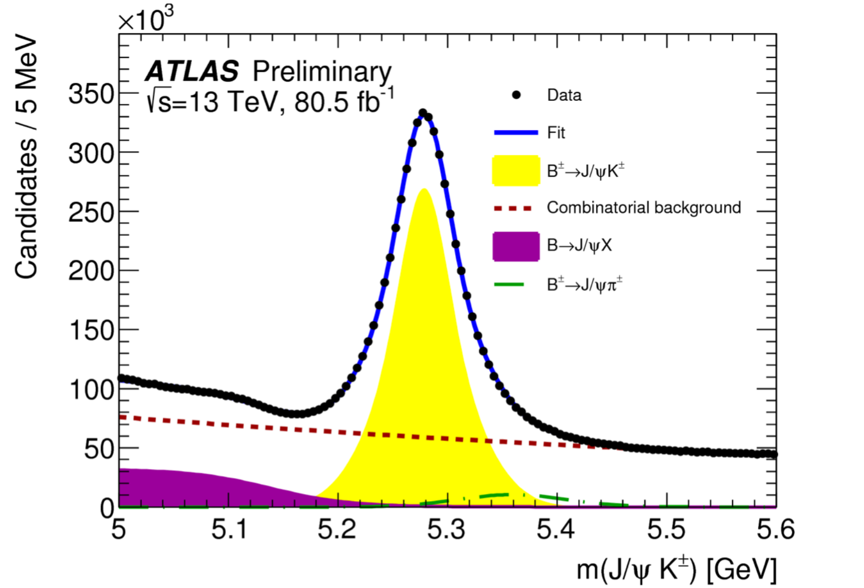

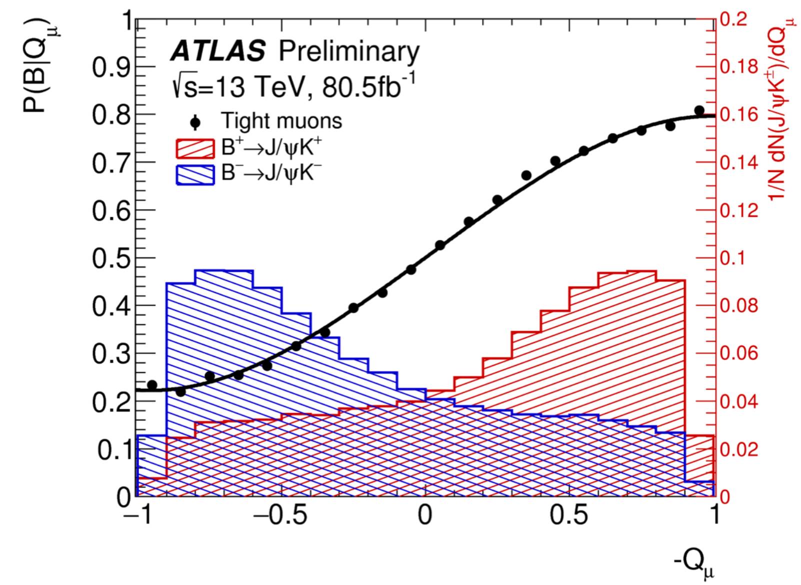

Measured B_s^0 Properties

- The B_s^0 mass fit and the proper decay time fit are shown here

$$t = \frac{L_{xy}\, m_B}{p_{\mathrm{T}_B}}$$

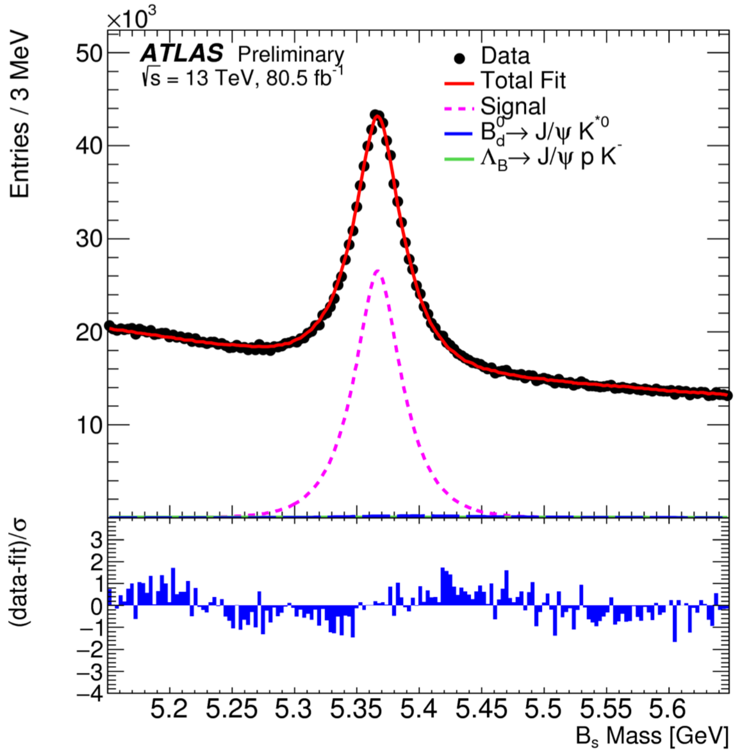

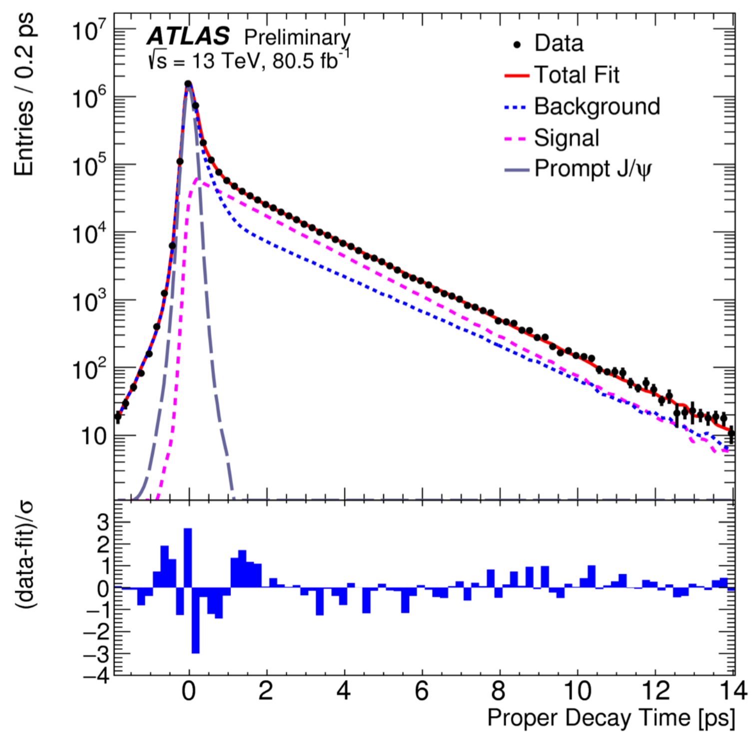

- The measured transversity angles, θ_T, ϕ_T, and ψ_T are shown here

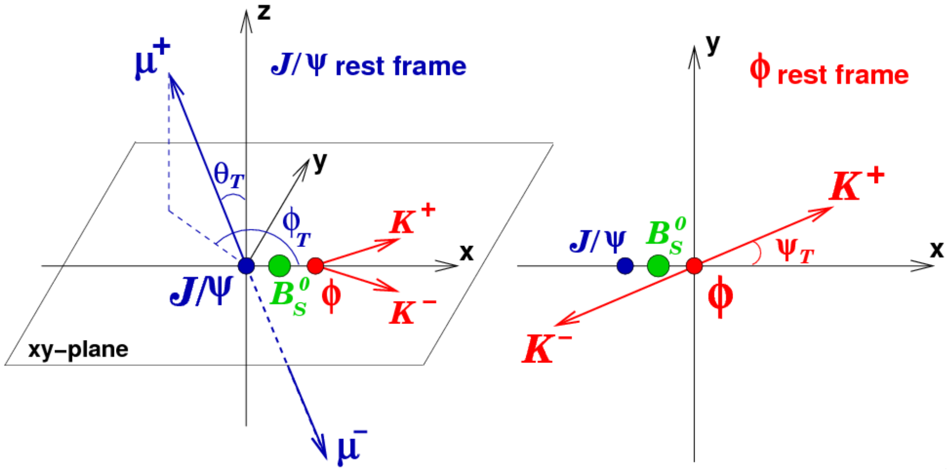

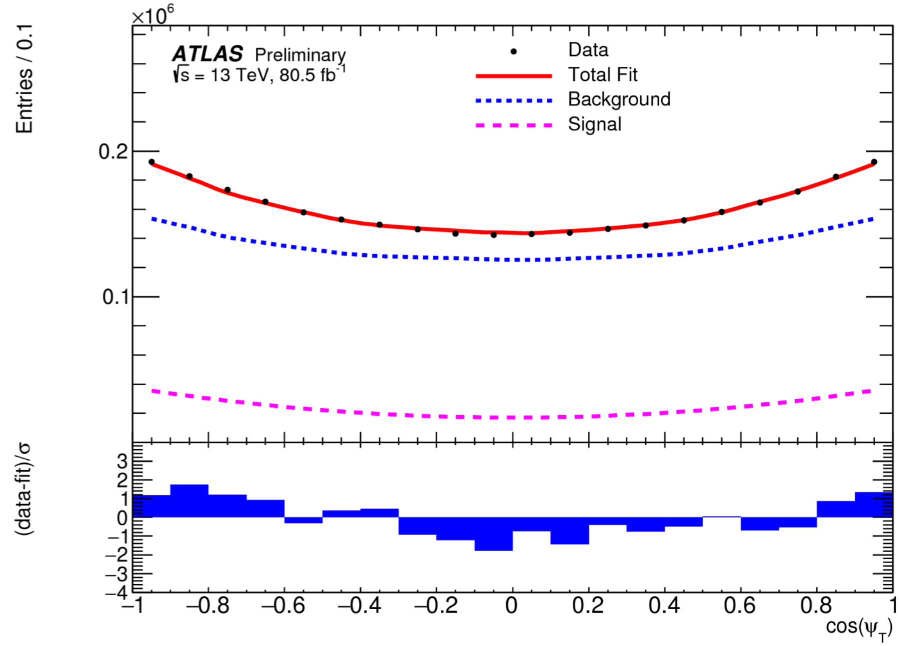

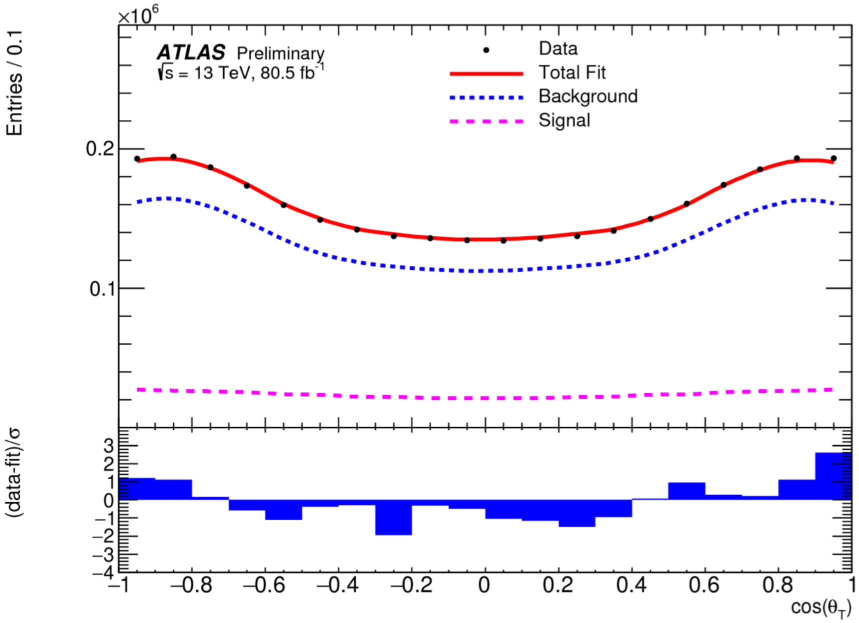

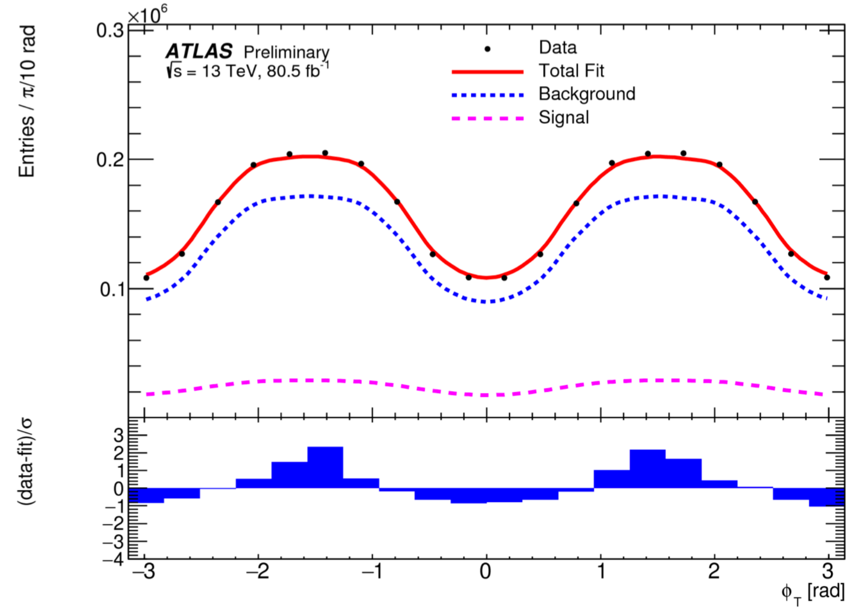

Run 2 Results

- The Run 2 results with 80.5 fb^{-1} of data are shown in the table on the left
- The combined Run 1 and Run 2 results are shown in the red circle in the figure on the right

Parameter	Value	Statistical uncertainty	Systematic uncertainty
ϕ_s[rad]	–0.068	0.038	0.018
$\Delta\Gamma_s$[ps^{-1}]	0.067	0.005	0.002
Γ_s[ps^{-1}]	0.669	0.001	0.001
$\|A_{\|\|}(0)\|^2$	0.219	0.002	0.002
$\|A_0(0)\|^2$	0.517	0.001	0.004
$\|A_S(0)\|^2$	0.046	0.003	0.004
$\delta_\perp$ [rad]	2.946	0.101	0.097
$\delta_{\|\|}$ [rad]	3.267	0.082	0.201
$\delta_\perp - \delta_S$ [rad]	–0.220	0.037	0.010

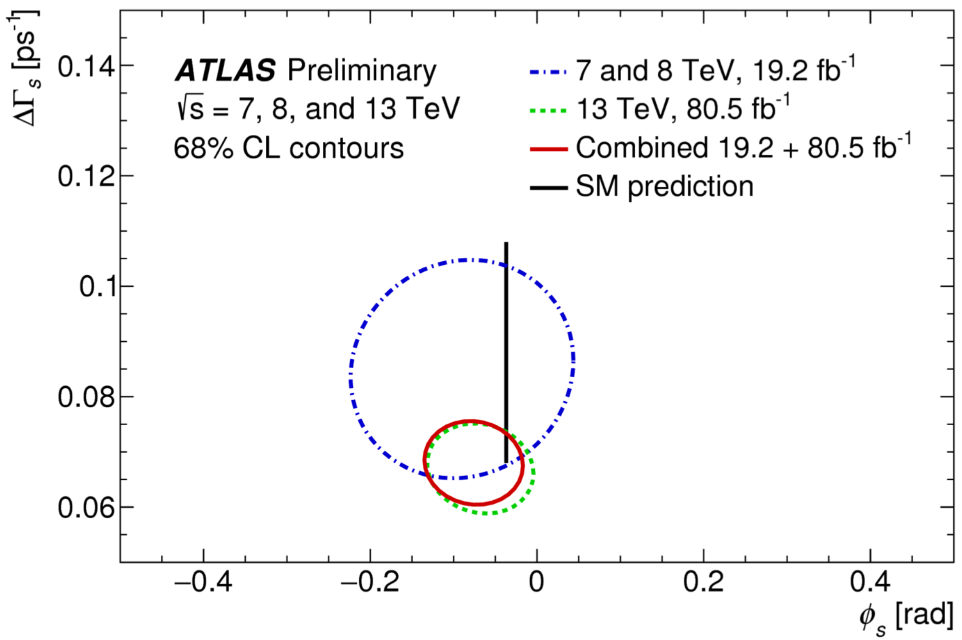

Combination Results

- The combined Run 1 and Run 2 results are shown in the table to the left
- The preliminary HFLAV average combination of the best experimental results is shown in the figure on the right

Parameter	Value	Statistical uncertainty	Systematic uncertainty
ϕ_s[rad]	–0.076	0.034	0.019
$\Delta\Gamma_s[\mathrm{ps}^{-1}]$	0.068	0.004	0.003
$\Gamma_s[\mathrm{ps}^{-1}]$	0.669	0.001	0.001
$\|A_\parallel(0)\|^2$	0.220	0.002	0.002
$\|A_0(0)\|^2$	0.517	0.001	0.004
$\|A_S\|^2$	0.043	0.004	0.004
$\delta_\perp$ [rad]	3.075	0.096	0.091
$\delta_\parallel$ [rad]	3.295	0.079	0.202
$\delta_\perp - \delta_S$ [rad]	–0.216	0.037	0.010

Preliminary HFLAV average, F. Dordei, CERN seminar 2019-05-07

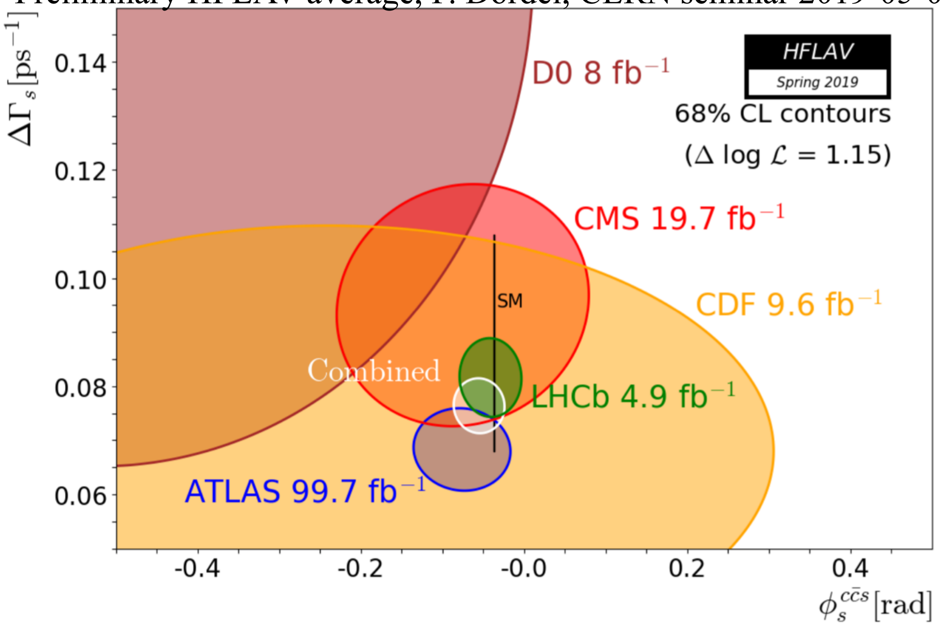

$B_s^0 \to J/\psi\phi$ CP Violation Projections

- HL-LHC projections of the CP violation phase and decay width difference are shown here.
- With higher statistics due to trigger selection the precision of the result will improve

Zoomed in view:

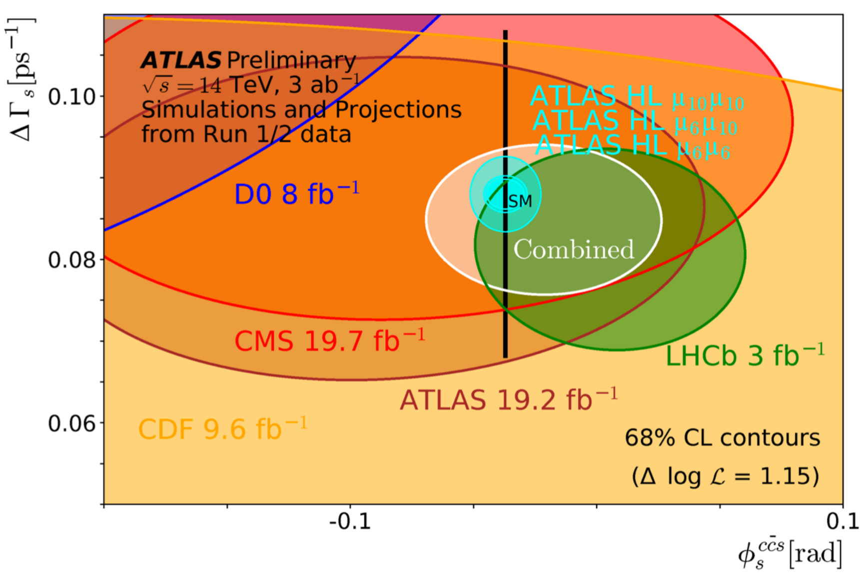

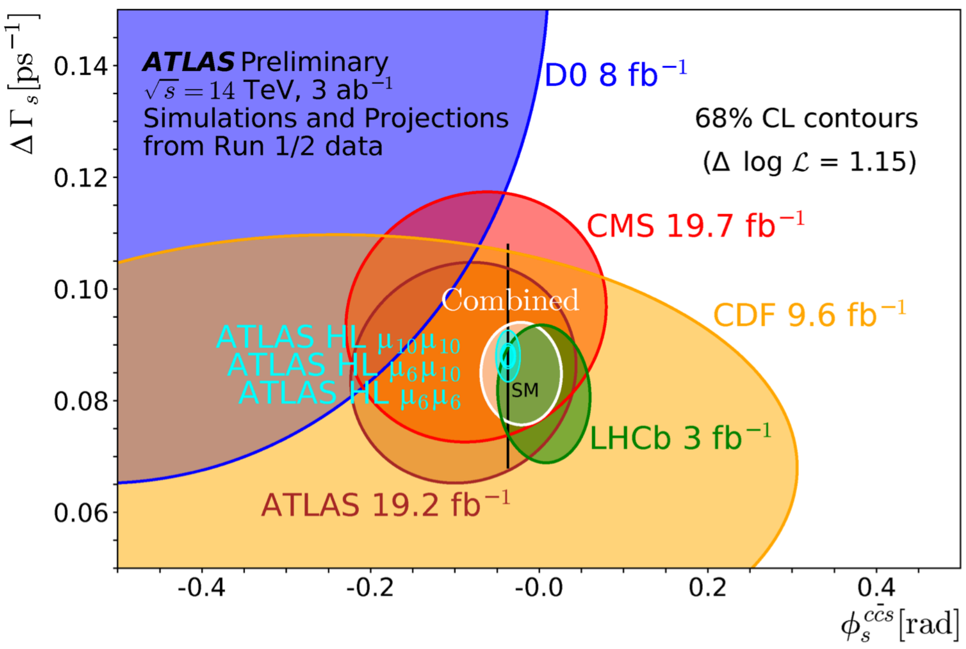

Final Remarks

- The combined ATLAS results from Run 1 and the 2015 and 2016 results of the $B^0_{(s)} \rightarrow \mu^+\mu^-$ analysis were presented
  - The results are compatible with the Standard Model within 2.4σ
- The combined ATLAS results from Run 1 and the 2015, 2016, and 2017 results of the CP Violation in $B^0_s \rightarrow J/\psi\phi$ were presented
  - The result is the most stringent measurement on parameters ϕ_s, $\Delta\Gamma_s$, Γ_s and the helicity functions parameters of the $B^0_s \rightarrow J/\psi\phi$ decay from a single measurement
- With the HL-LHC statistics, more precise measurements will be possible

Additional Slides

- The following slides provide supplementary and follow up material to the presentation

Description of BDT Variables

Variable	Description
p_{T}^{B}	Magnitude of the B candidate transverse momentum $\overrightarrow{p_{\mathrm{T}}}^{B}$.
$\chi^2_{\mathrm{PV,DV}\ xy}$	Compatibility of the separation $\overrightarrow{\Delta x}$ between production (*i.e.* associated PV) and decay (DV) vertices in the transverse projection: $\overrightarrow{\Delta x}_{\mathrm{T}} \cdot \Sigma^{-1}_{\overrightarrow{\Delta x}_{\mathrm{T}}} \cdot \overrightarrow{\Delta x}_{\mathrm{T}}$, where $\Sigma_{\overrightarrow{\Delta x}_{\mathrm{T}}}$ is the covariance matrix.
ΔR	three-dimensional opening between $\overrightarrow{p}^{B}$ and $\overrightarrow{\Delta x}$: $\sqrt{\alpha_{\mathrm{2D}}{}^2 + \Delta\eta^2}$
$\lvert\alpha_{\mathrm{2D}}\rvert$	Absolute value of the angle between $\overrightarrow{p_{\mathrm{T}}}^{B}$ and $\overrightarrow{\Delta x}_{\mathrm{T}}$ (transverse projection).
L_{xy}	Projection of $\overrightarrow{\Delta x}_{\mathrm{T}}$ along the direction of $\overrightarrow{p}_{\mathrm{T}}^{B}$: $(\overrightarrow{\Delta x}_{\mathrm{T}} \cdot \overrightarrow{p_{\mathrm{T}}}^{B})/\lvert\overrightarrow{p_{\mathrm{T}}}^{B}\rvert$.
$\mathrm{IP}_{B}^{\mathrm{3D}}$	three-dimensional impact parameter of the B candidate to the associated PV.
$\mathrm{DOCA}_{\mu\mu}$	Distance of closest approach (DOCA) of the two tracks forming the B candidate (three-dimensional).
$\Delta\phi_{\mu\mu}$	Difference in azimuthal angle between the momenta of the two tracks forming the B candidate.
$\lvert d_0\rvert^{\mathrm{max}}$-sig.	Significance of the larger absolute value of the impact parameters to the PV of the tracks forming the B candidate, in the transverse plane.
$\lvert d_0\rvert^{\mathrm{min}}$-sig.	Significance of the smaller absolute value of the impact parameters to the PV of the tracks forming the B candidate, in the transverse plane.
$P_{\mathrm{L}}^{\mathrm{min}}$	Value of the smaller projection of the momenta of the muon candidates along $\overrightarrow{p_{\mathrm{T}}}^{B}$.
$I_{0.7}$	Isolation variable defined as ratio of $\lvert\overrightarrow{p_{\mathrm{T}}}^{B}\rvert$ to the sum of $\lvert\overrightarrow{p_{\mathrm{T}}}^{B}\rvert$ and of the transverse momenta of all additional tracks contained within a cone of size $\Delta R < 0.7$ around the B direction. Only tracks matched to the same PV as the B candidate are included in the sum.
$\mathrm{DOCA}_{\mathrm{xtrk}}$	DOCA of the closest additional track to the decay vertex of the B candidate. Tracks matched to a PV different from the B candidate are excluded.
$N_{\mathrm{xtrk}}^{\mathrm{close}}$	Number of additional tracks compatible with the decay vertex (DV) of the B candidate with $\ln(\chi^2_{\mathrm{xtrk,DV}}) < 1$. The tracks matched to a PV different from the B candidate are excluded.
$\chi^2_{\mu,\mathrm{xPV}}$	Minimum χ^2 for the compatibility of a muon in the B candidate with any PV reconstructed in the event.

Calculation of the Branching Ratio

- Each piece of the branching ratio is now obtained:
  - $N_s = 80 \pm 22$ and $N_d = -12 \pm 20$
  - $R_\varepsilon = \frac{\varepsilon(B^+ \to J/\psi\, K^+)}{\varepsilon(B^0_{(s)} \to \mu^+\mu^-)} = 0.1176 \pm 0.0009$ (stat.) $\pm\, 0.0047$ (syst.)
  - $N_{J/\psi K^+} = 334351$ with a statistical uncertainty of 0.3%
  - $\mathcal{B}(B^+ \to J/\psi K^+) = (1.010 \pm 0.029) \times 10^{-3}$
  - $\mathcal{B}(J/\psi \to \mu^+\mu^-) = (5.961 \pm 0.033)\%$
  - $f_s/f_d = 0.256 \pm 0.013$ (HFLAV average *)

$$\mathcal{B}(B^0_{(s)} \to \mu^+\mu^-) = \frac{N_{d(s)}}{\varepsilon_{\mu^+\mu^-}} \times [\mathcal{B}(B^+ \to J/\psi\, K^+) \times \mathcal{B}(J/\psi \to \mu^+\mu^-)]\, \frac{\varepsilon_{J/\psi K^+}}{N_{J/\psi K^+}} \times \frac{f_u}{f_{d(s)}}$$

*HFLAV collaboration, Averages of *b*-hadron, *c*-hadron and τ-lepton properties as of summer 2016, Eur. Phys. J. C 77 (2017) 895 [arXiv:1612.07233]

Decision Trees

- A machine learning algorithm can be taught to make predictions based on experience with example datasets.
- This machine learning approach is called classification
- Obtaining a probability that an event is either background or signal

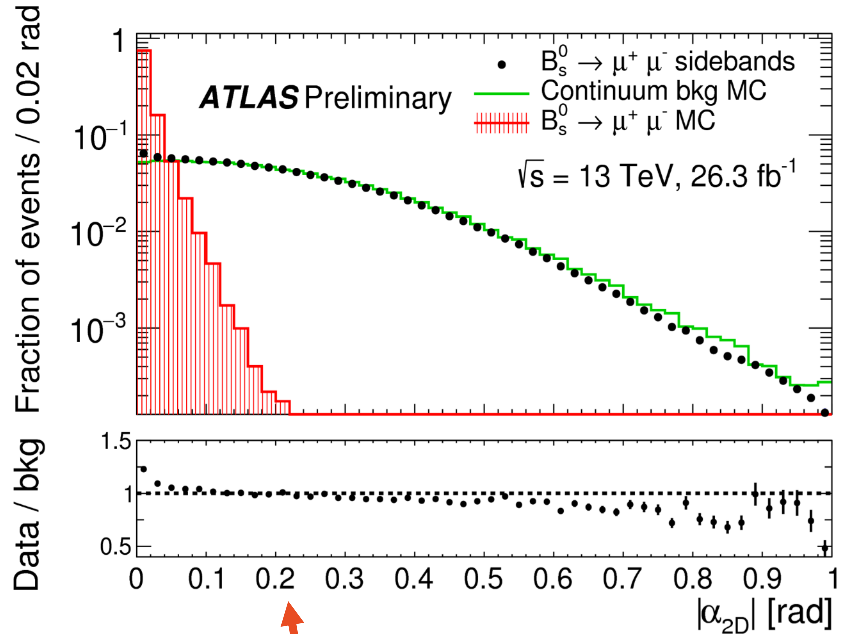

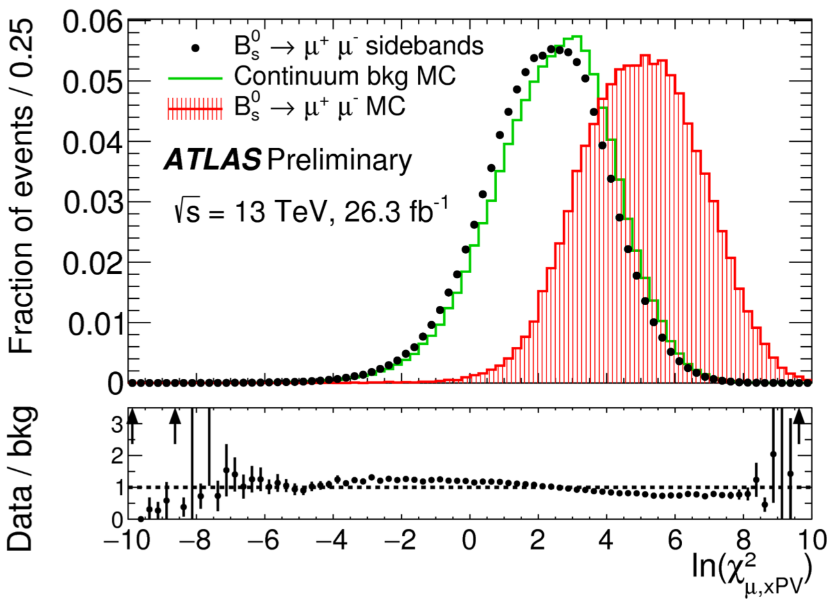

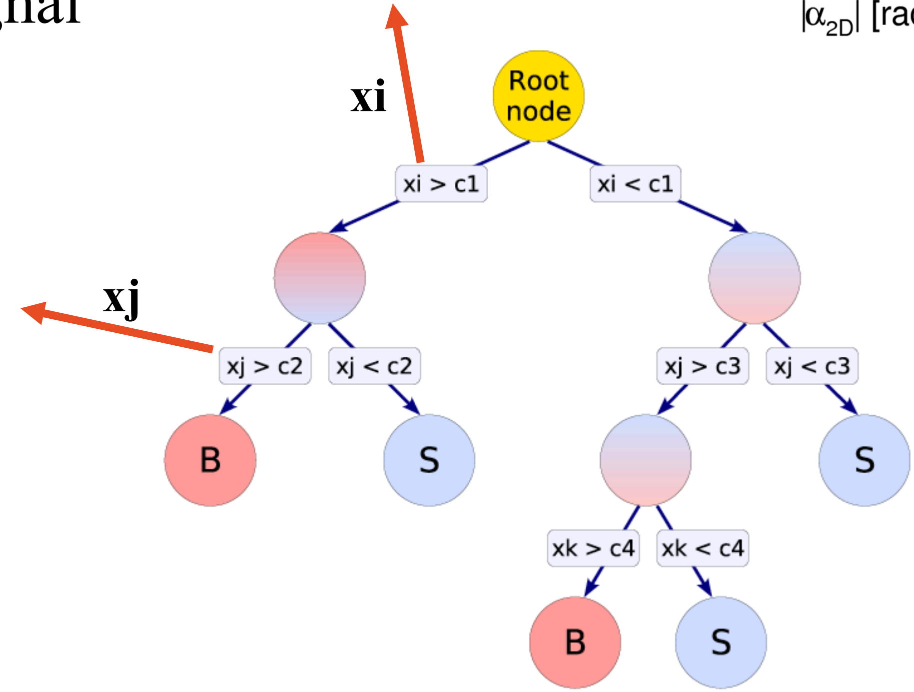

- The sidebands and the signal Monte Carlo are used for the BDT training
- The sample is subdivided into three randomly selected separate and equally populated sub-samples
- These samples are used in rotation to train, verify, and evaluate the selection efficiency of 3 individual BDTs

- The 3 BDTs produce statistically compatible performances
- They are then combined into one single classifier in such a way that each BDT is applied only to the part of the data sample not involved in the BDT training.

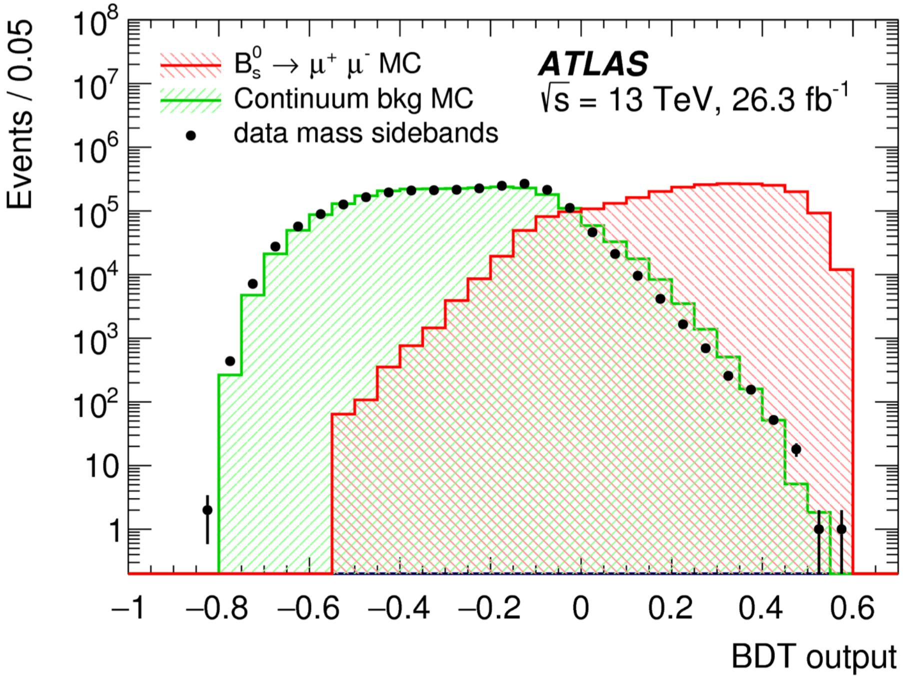

Comparison of Sidebands and Simulation

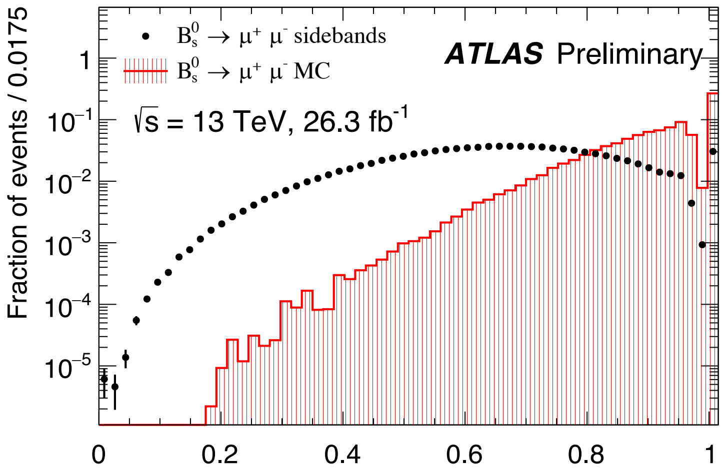

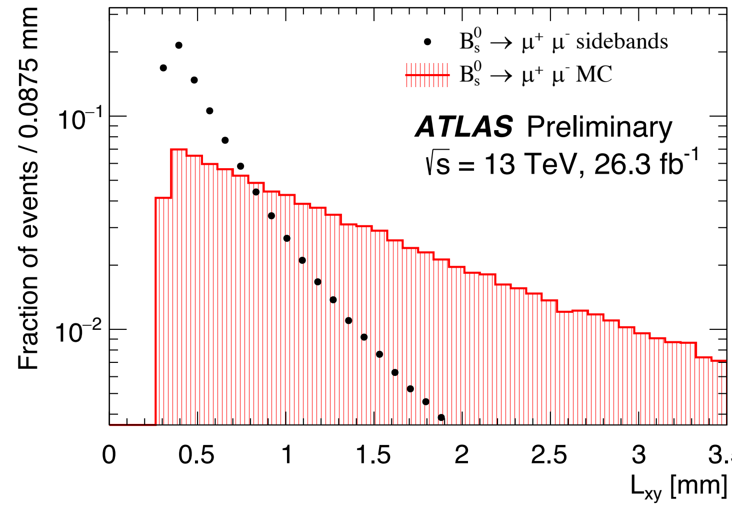

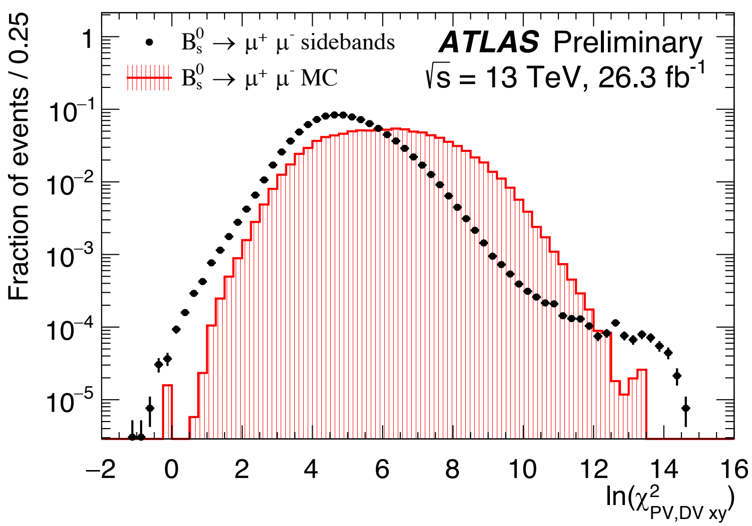

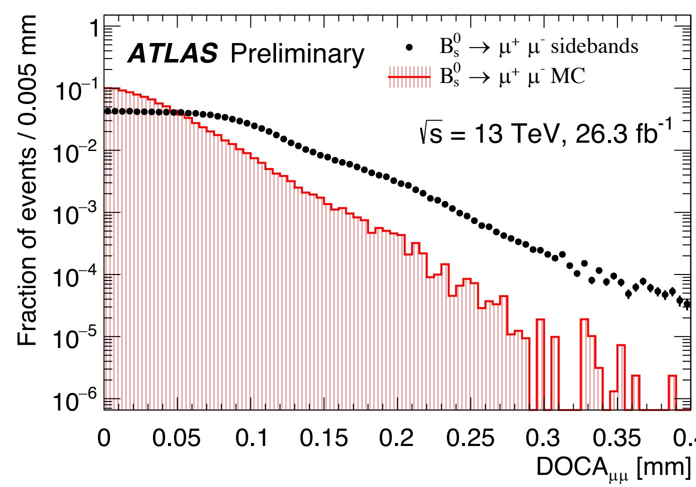

Correlation of Variables Before the BDT Selection

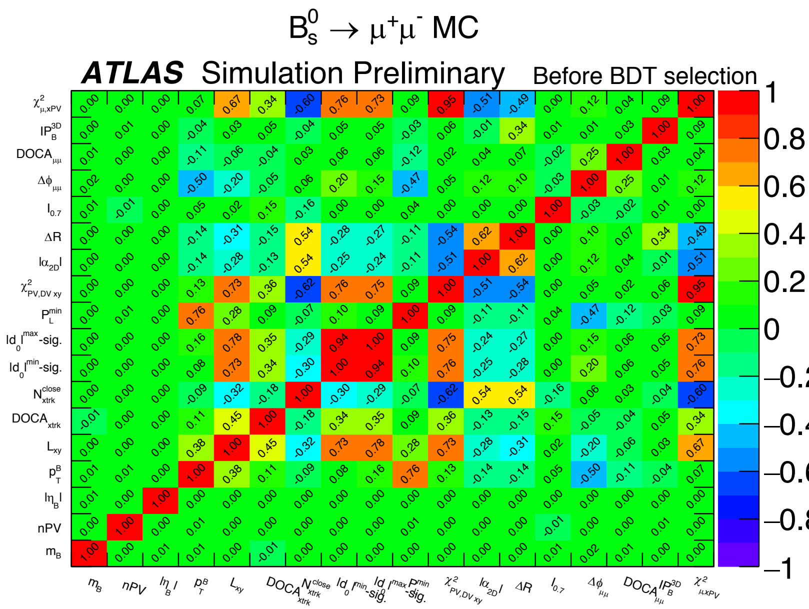

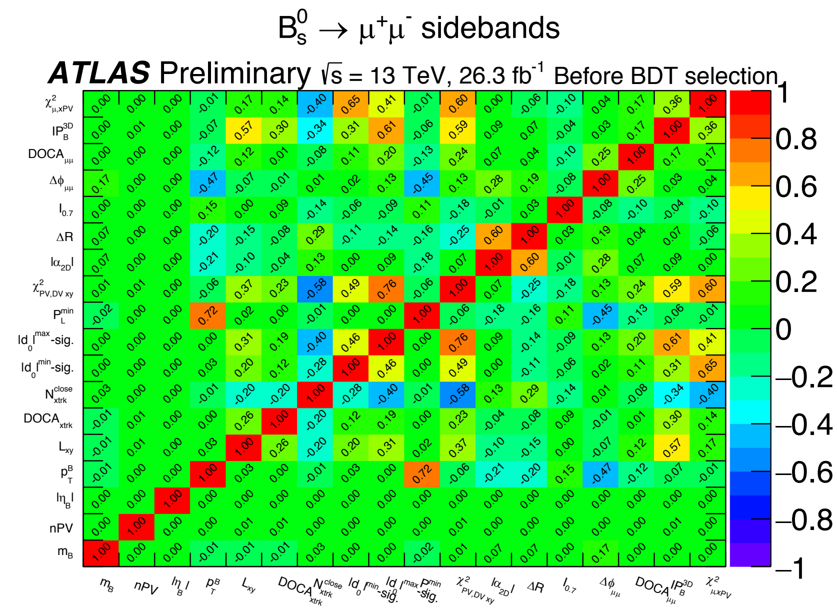

Correlation of Variables After the BDT Selection

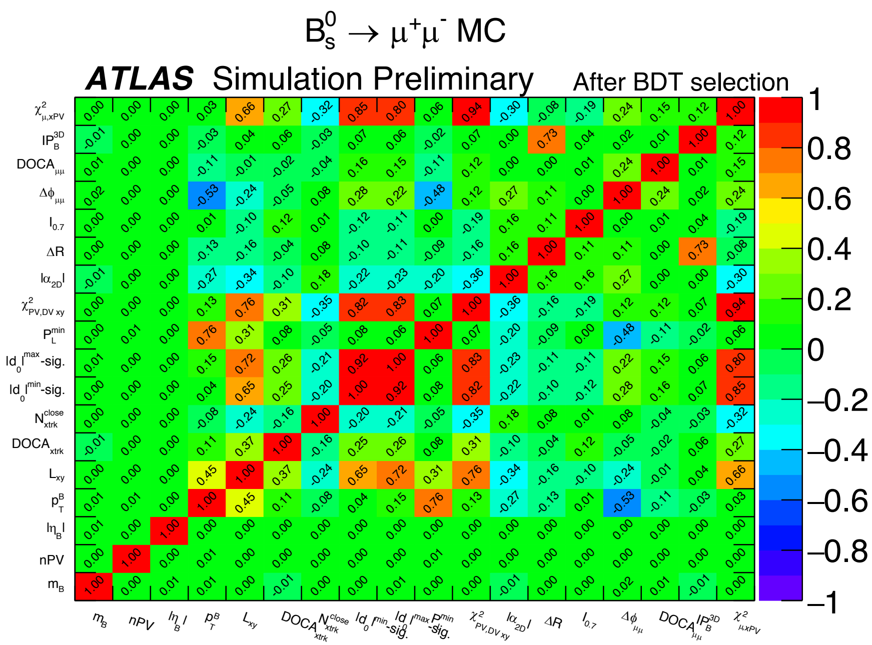

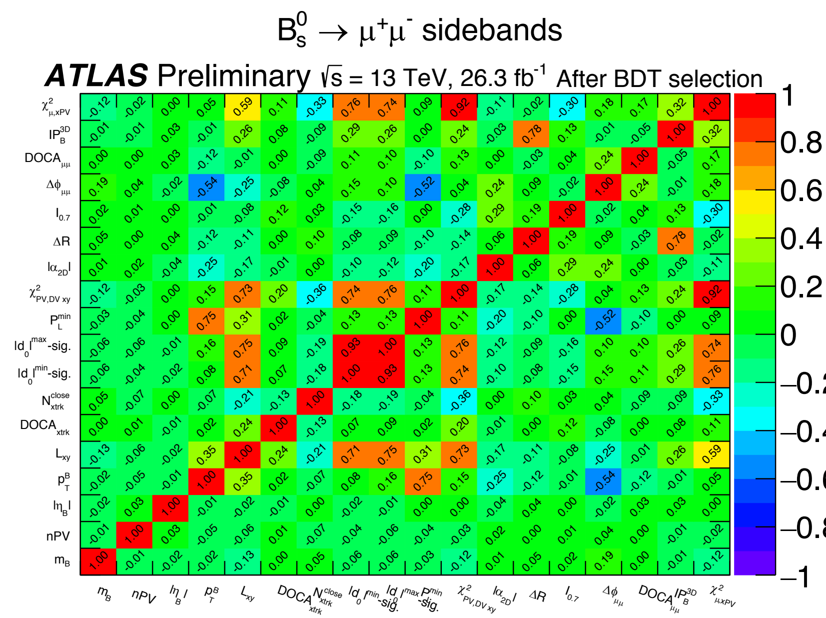

Comment on Negative Likelihood Values

- The central value of the maximum likelihood fit is allowed to be negative as a consequence of this particular statistical observable. We know that a negative value is not physical for the number of events N_d in the branching fraction and also the branching fraction of Bd. Because we know that a negative value is not physical we can use a robust statistical tool called the Neyman construction to find an upper bound on Nd. The Neyman construction takes as input the measured branching ratios for Bs and Bd from the maximum likelihood and returns the possible number of events Nd and Ns. A feature of the Neyman construction is that it cannot return negative values for Nd or Ns.
- In the end we quote a measurement for BR(Bs) and an upper limit for BR(Bd). These are calculated from the output of the Nd and Ns belts in the Neyman construction.

$B_s^0 \to \mathrm{J}/\psi\phi$

- Differential decay rate: $\dfrac{\mathrm{d}^4\Gamma}{\mathrm{d}t\ \mathrm{d}\Omega} = \sum_{k=1}^{10} O^{(k)}(t) g^{(k)}(\theta_T, \psi_T, \phi_T)$

Table 4: The ten time-dependent functions, $O^{(k)}(t)$ and the functions of the transversity angles $g^{(k)}(\theta_T, \psi_T, \phi_T)$. The amplitudes $|A_0(0)|^2$ and $|A_\parallel(0)|^2$ are for the CP-even components of the $B_s^0 \to J/\psi\phi$ decay, $|A_\perp(0)|^2$ is the CP-odd amplitude; they have corresponding strong phases δ_0, $\delta_\parallel$ and $\delta_\perp$. By convention δ_0 is set to be zero. The S–wave amplitude $|A_S(0)|^2$ gives the fraction of $B_s^0 \to J/\psi K^+K^-(f_0)$ and has a related strong phase δ_S. The factor α is described in the text of Section 5.1. The $\pm$ and $\mp$ terms denote two cases: the upper sign describes the decay of a meson that was initially a B_s^0 meson, while the lower sign describes the decays of a meson that was initially $\bar{B}_s^0$.

k	$O^{(k)}(t)$	$g^{(k)}(\theta_T, \psi_T, \phi_T)$
1	$\frac{1}{2}\|A_0(0)\|^2 \left[(1+\cos\phi_s)\, e^{-\Gamma_L^{(s)}t} + (1-\cos\phi_s)\, e^{-\Gamma_H^{(s)}t} \pm 2e^{-\Gamma_s t}\sin(\Delta m_s t)\sin\phi_s\right]$	$2\cos^2\psi_T(1-\sin^2\theta_T\cos^2\phi_T)$
2	$\frac{1}{2}\|A_\parallel(0)\|^2 \left[(1+\cos\phi_s)\, e^{-\Gamma_L^{(s)}t} + (1-\cos\phi_s)\, e^{-\Gamma_H^{(s)}t} \pm 2e^{-\Gamma_s t}\sin(\Delta m_s t)\sin\phi_s\right]$	$\sin^2\psi_T(1-\sin^2\theta_T\sin^2\phi_T)$
3	$\frac{1}{2}\|A_\perp(0)\|^2 \left[(1-\cos\phi_s)\, e^{-\Gamma_L^{(s)}t} + (1+\cos\phi_s)\, e^{-\Gamma_H^{(s)}t} \mp 2e^{-\Gamma_s t}\sin(\Delta m_s t)\sin\phi_s\right]$	$\sin^2\psi_T\sin^2\theta_T$
4	$\frac{1}{2}\|A_0(0)\|\|A_\parallel(0)\|\cos\delta_{\|\|}$ $\left[(1+\cos\phi_s)\, e^{-\Gamma_L^{(s)}t} + (1-\cos\phi_s)\, e^{-\Gamma_H^{(s)}t} \pm 2e^{-\Gamma_s t}\sin(\Delta m_s t)\sin\phi_s\right]$	$\frac{1}{\sqrt{2}}\sin 2\psi_T\sin^2\theta_T\sin 2\phi_T$
5	$\|A_\parallel(0)\|\|A_\perp(0)\|[\frac{1}{2}(e^{-\Gamma_L^{(s)}t} - e^{-\Gamma_H^{(s)}t})\cos(\delta_\perp - \delta_{\|\|})\sin\phi_s$ $\pm e^{-\Gamma_s t}(\sin(\delta_\perp - \delta_\parallel)\cos(\Delta m_s t) - \cos(\delta_\perp - \delta_\parallel)\cos\phi_s\sin(\Delta m_s t))]$	$-\sin^2\psi_T\sin 2\theta_T\sin\phi_T$
6	$\|A_0(0)\|\|A_\perp(0)\|[\frac{1}{2}(e^{-\Gamma_L^{(s)}t} - e^{-\Gamma_H^{(s)}t})\cos\delta_\perp\sin\phi_s$ $\pm e^{-\Gamma_s t}(\sin\delta_\perp\cos(\Delta m_s t) - \cos\delta_\perp\cos\phi_s\sin(\Delta m_s t))]$	$\frac{1}{\sqrt{2}}\sin 2\psi_T\sin 2\theta_T\cos\phi_T$
7	$\frac{1}{2}\|A_S(0)\|^2 \left[(1-\cos\phi_s)\, e^{-\Gamma_L^{(s)}t} + (1+\cos\phi_s)\, e^{-\Gamma_H^{(s)}t} \mp 2e^{-\Gamma_s t}\sin(\Delta m_s t)\sin\phi_s\right]$	$\frac{2}{3}(1-\sin^2\theta_T\cos^2\phi_T)$
8	$\alpha\|A_S(0)\|\|A_\parallel(0)\|[\frac{1}{2}(e^{-\Gamma_L^{(s)}t} - e^{-\Gamma_H^{(s)}t})\sin(\delta_\parallel - \delta_S)\sin\phi_s$ $\pm e^{-\Gamma_s t}(\cos(\delta_\parallel - \delta_S)\cos(\Delta m_s t) - \sin(\delta_\parallel - \delta_S)\cos\phi_s\sin(\Delta m_s t))]$	$\frac{1}{3}\sqrt{6}\sin\psi_T\sin^2\theta_T\sin 2\phi_T$
9	$\frac{1}{2}\alpha\|A_S(0)\|\|A_\perp(0)\|\sin(\delta_\perp - \delta_S)$ $\left[(1-\cos\phi_s)\, e^{-\Gamma_L^{(s)}t} + (1+\cos\phi_s)\, e^{-\Gamma_H^{(s)}t} \mp 2e^{-\Gamma_s t}\sin(\Delta m_s t)\sin\phi_s\right]$	$\frac{1}{3}\sqrt{6}\sin\psi_T\sin 2\theta_T\cos\phi_T$
10	$\alpha\|A_0(0)\|\|A_S(0)\|[\frac{1}{2}(e^{-\Gamma_H^{(s)}t} - e^{-\Gamma_L^{(s)}t})\sin\delta_S\sin\phi_s$ $\pm e^{-\Gamma_s t}(\cos\delta_S\cos(\Delta m_s t) + \sin\delta_S\cos\phi_s\sin(\Delta m_s t))]$	$\frac{4}{3}\sqrt{3}\cos\psi_T\,(1-\sin^2\theta_T\cos^2\phi_T)$

$$B_d^0 \rightarrow K^{*0}(892)\mu^+\mu^-$$

$B_d^0 \to K^{*0}(892)\mu^+\mu^-$

- differential decay rate as a function of the angular parameters

$$\frac{1}{\mathrm{d}\Gamma/\mathrm{d}q^2}\frac{\mathrm{d}^4\Gamma}{\mathrm{d}\cos\theta_L\,\mathrm{d}\cos\theta_K\,\mathrm{d}\phi\,\mathrm{d}q^2} = \frac{9}{32\pi}\Bigg[\frac{3(1-F_L)}{4}\sin^2\theta_K + F_L\cos^2\theta_K + \frac{1-F_L}{4}\sin^2\theta_K\cos 2\theta_L \\ - F_L\cos^2\theta_K\cos 2\theta_L + S_3\sin^2\theta_K\sin^2\theta_L\cos 2\phi \\ + S_4\sin 2\theta_K\sin 2\theta_L\cos\phi + S_5\sin 2\theta_K\sin\theta_L\cos\phi \\ + S_6\sin^2\theta_K\cos\theta_L + S_7\sin 2\theta_K\sin\theta_L\sin\phi \\ + S_8\sin 2\theta_K\sin 2\theta_L\sin\phi + S_9\sin^2\theta_K\sin^2\theta_L\sin 2\phi\Bigg]. \qquad (2.1)$$

$$P_1 = \frac{2S_3}{1-F_L}$$

$$P_2 = \frac{2}{3}\frac{A_{\mathrm{FB}}}{1-F_L}$$

$$P_3 = -\frac{S_9}{1-F_L}$$

$$P'_{j=4,5,6,8} = \frac{S_{i=4,5,7,8}}{\sqrt{F_L(1-F_L)}}.$$

Angular Analysis $B_d^0 \to K^*\mu^+\mu^-$

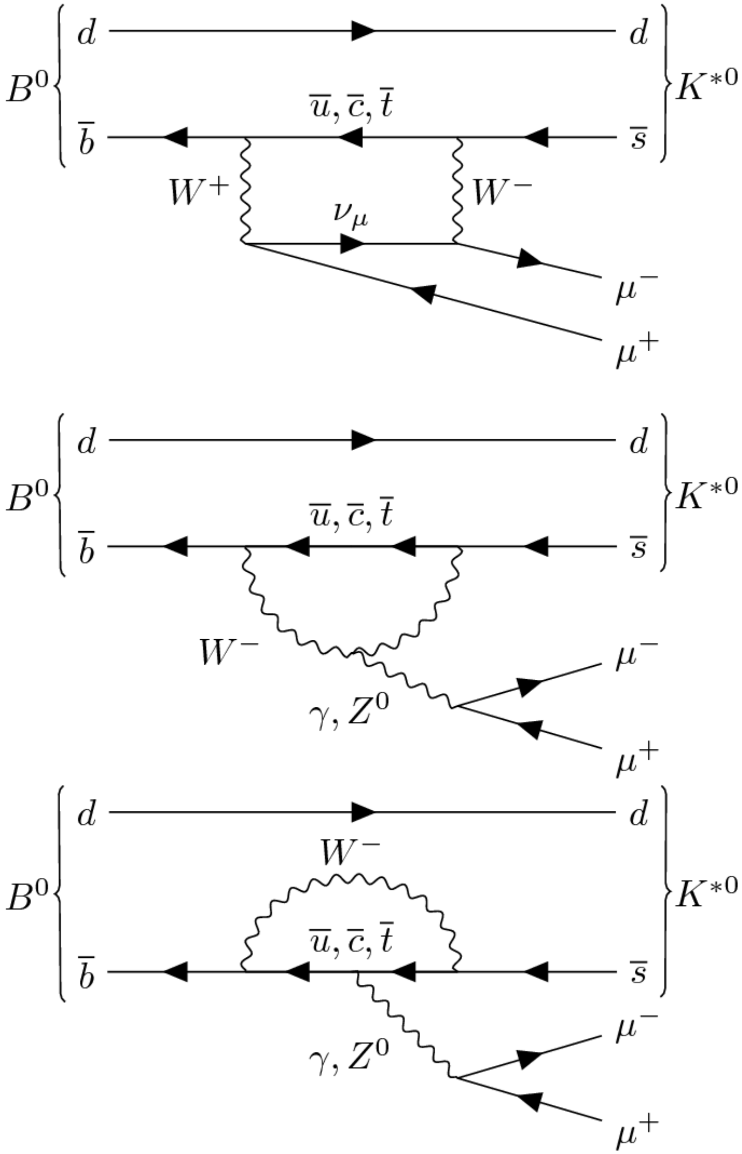

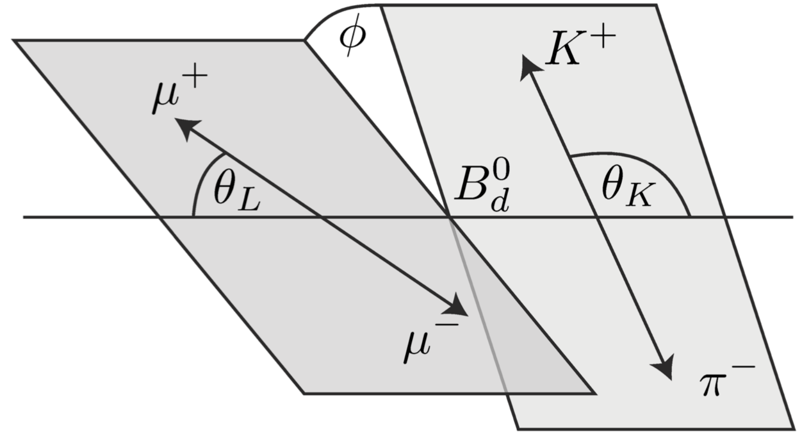

$B_d^0 \to K^*(\to K^+\pi^-)\,\mu^+\mu^-$

- Search for heavy new particles that may contribute to FCNC decay amplitudes
- The lowest order Feynman diagrams for $B_d^0 \to K^*\mu^+\mu^-$ are the box diagram shown on the upper left and the two penguin diagrams
- The angular parameters of the measurement are shown in the upper right diagram in the rest frame of the K^*

Analysis Scheme

- The differential decay amplitude of $B_d^0 \to K^* \mu^+ \mu^-$ can be written in terms of:
  - $q^2 = 4m_\mu^2$, $\cos(\theta_K)$, $\cos(\theta_L)$ and ϕ
  - The fraction of longitudinally polarized K^* mesons (F_L)
  - And 7 angular coefficients, S_i where i = 3,4,5,6,7,8,9
  - Theoretical uncertainties can be reduced in the decay amplitude using ratios of F_L and S_i to form P_1, P_2, P_3 and P_j' where j = 4,5,6,8
- The equation can be simplified using trigonometric transformations to "fold" certain angular distributions so that only 3 coefficients remain in the decay amplitude

Folding Schemes:

$$F_L, S_3, S_4, P_4' : \begin{cases} \phi \to -\phi & \text{for } \phi < 0 \\ \phi \to \pi - \phi & \text{for } \theta_L > \frac{\pi}{2} \\ \theta_L \to \pi - \theta_L & \text{for } \theta_L > \frac{\pi}{2}, \end{cases}$$

$$F_L, S_3, S_5, P_5' : \begin{cases} \phi \to -\phi & \text{for } \phi < 0 \\ \theta_L \to \pi - \theta_L & \text{for } \theta_L > \frac{\pi}{2}, \end{cases}$$

$$F_L, S_3, S_7, P_6' : \begin{cases} \phi \to \pi - \phi & \text{for } \phi > \frac{\pi}{2} \\ \phi \to -\pi - \phi & \text{for } \phi < -\frac{\pi}{2} \\ \theta_L \to \pi - \theta_L & \text{for } \theta_L > \frac{\pi}{2}, \end{cases}$$

$$F_L, S_3, S_8, P_8' : \begin{cases} \phi \to \pi - \phi & \text{for } \phi > \frac{\pi}{2} \\ \phi \to -\pi - \phi & \text{for } \phi < -\frac{\pi}{2} \\ \theta_L \to \pi - \theta_L & \text{for } \theta_L > \frac{\pi}{2} \\ \theta_K \to \pi - \theta_K & \text{for } \theta_L > \frac{\pi}{2}. \end{cases}$$

Resulting angular variable ranges:

$$\begin{aligned} &\cos\theta_L \in [0,1], \quad \cos\theta_K \in [-1,1] \quad \text{and} \quad \phi \in [0,\pi], \\ &\cos\theta_L \in [0,1], \quad \cos\theta_K \in [-1,1] \quad \text{and} \quad \phi \in [0,\pi], \\ &\cos\theta_L \in [0,1], \quad \cos\theta_K \in [-1,1] \quad \text{and} \quad \phi \in [-\pi/2,\pi/2], \\ &\cos\theta_L \in [0,1], \quad \cos\theta_K \in [-1,1] \quad \text{and} \quad \phi \in [-\pi/2,\pi/2], \end{aligned}$$

Extended Maximum Likelihood Fit

- An extended maximum likelihood fit process is used to extract the 3 coefficients of interest in a particular folding scheme:
  - F_{L}, S_3 and S_j where j = 4,5,7,8 (or F_{L}, S_3 and P_j' where j = 4,5,6,8)
  - Nuisance parameters (mass of $K\pi\mu\mu$ and mass width coefficient) are also extracted
- The fitting procedure is performed in 6 bins of q^2 between 0.04 and 6 GeV for each folding scheme in order to probe the dependence on q^2

Control Regions

- Two $K^*c\bar{c}$ decay control sample fits, K^*J/ψ and $K^*\psi(2S)$, are shown in $q^2 \in [8, 11]$ and $[12, 15]$ GeV^2 regions, respectively
- Control samples are used to extract values for nuisance parameters describing the signal
- The fit to data includes a combinatorial background component that does not peak in the $m_{K\pi\mu\mu}$ distribution

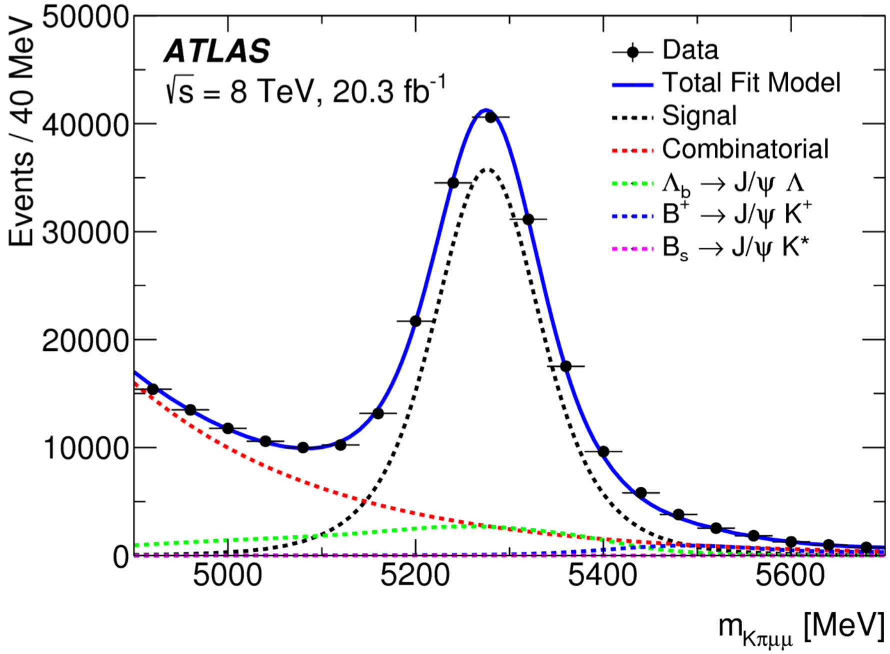

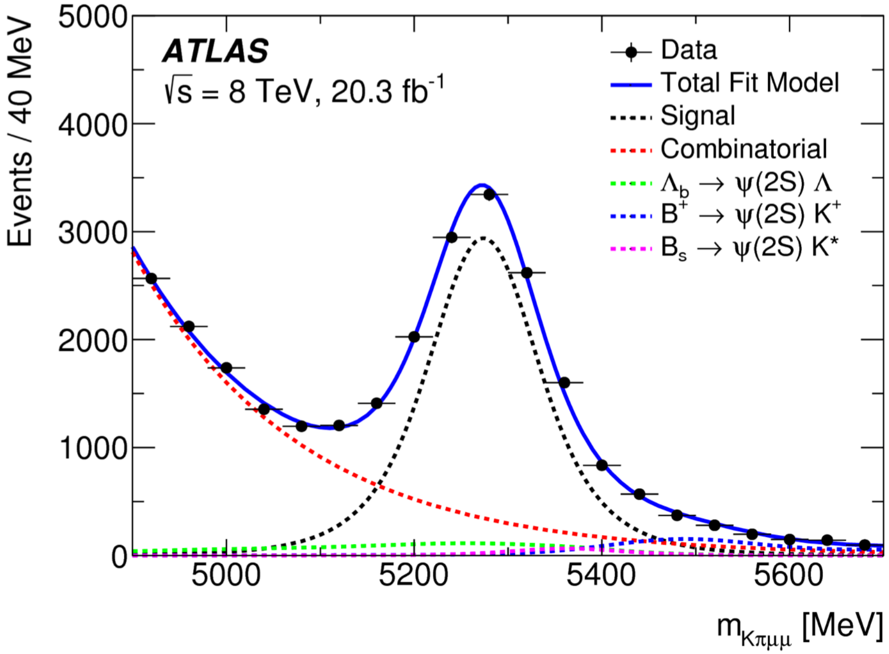

Subset of Results

- Fit to the mass $K\pi\mu\mu$ and angle ϕ in the dilepton mass region $q^2 \in [2.0, 4.0]$ GeV^2
- The fit is performed using the F_L, S_3 and S_5 folding scheme

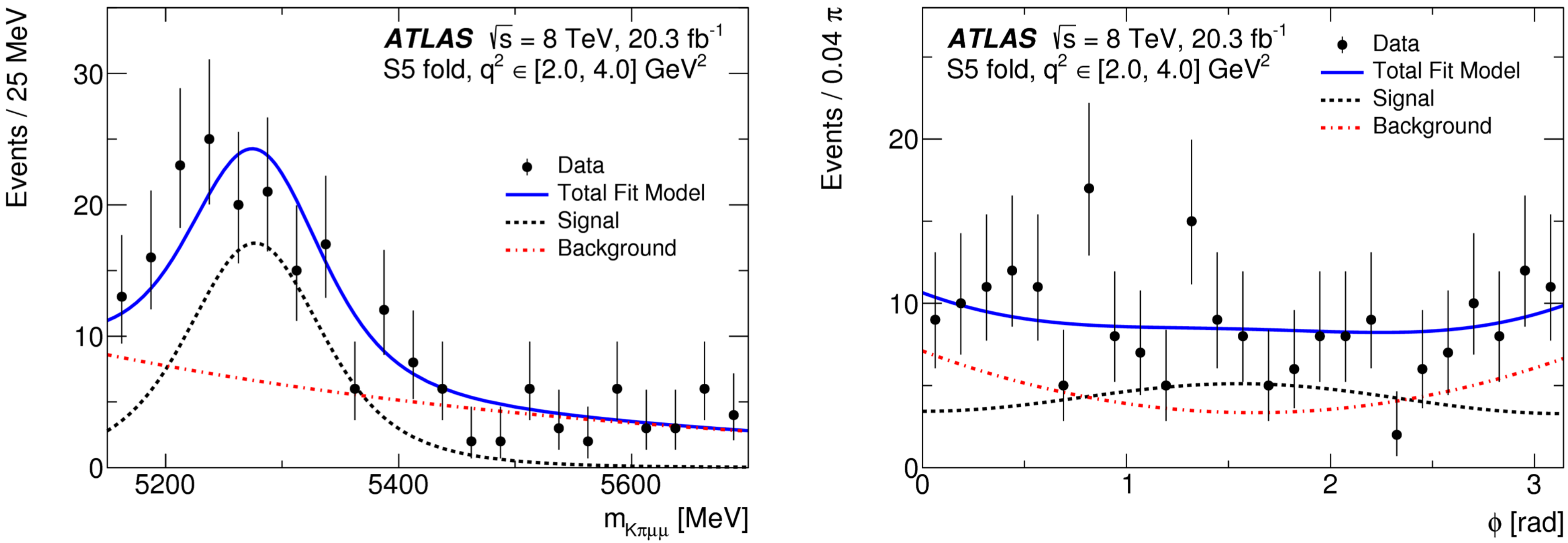

- Fitted signal and background yields are shown in the table for the various bins of q^2
- The fits to $\cos(\theta_K)$ and $\cos(\theta_L)$ in the $q^2 \in [2.0, 4.0]$ GeV^2 in the F_L, S_3 and S_5 folding scheme are shown here

q^2 [GeV^2]	n_{signal}	$n_{\mathrm{background}}$
[0.04, 2.0]	128 ± 22	122 ± 22
[2.0, 4.0]	106 ± 23	113 ± 23
[4.0, 6.0]	114 ± 24	204 ± 26
[0.04, 4.0]	236 ± 31	233 ± 32
[1.1, 6.0]	275 ± 35	363 ± 36
[0.04, 6.0]	342 ± 39	445 ± 40

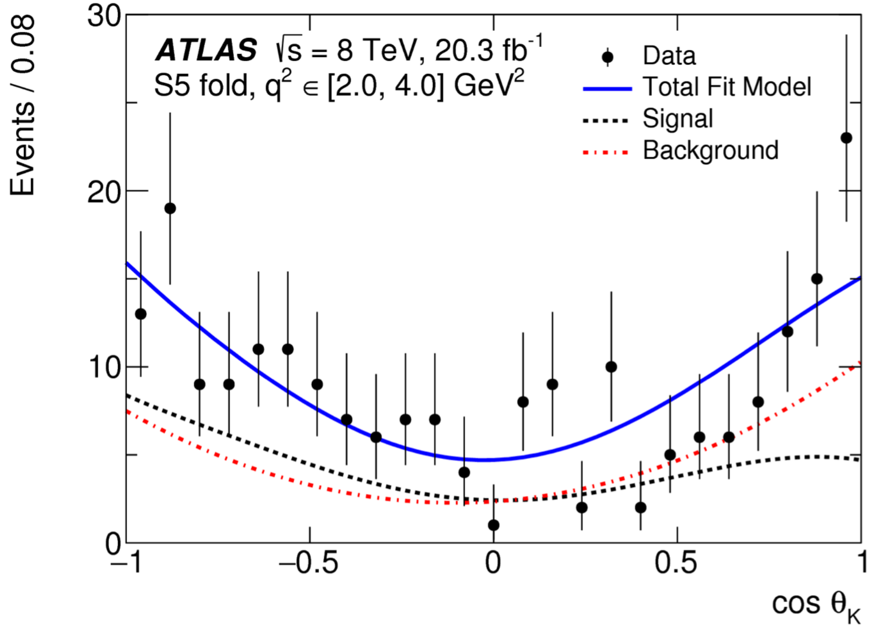

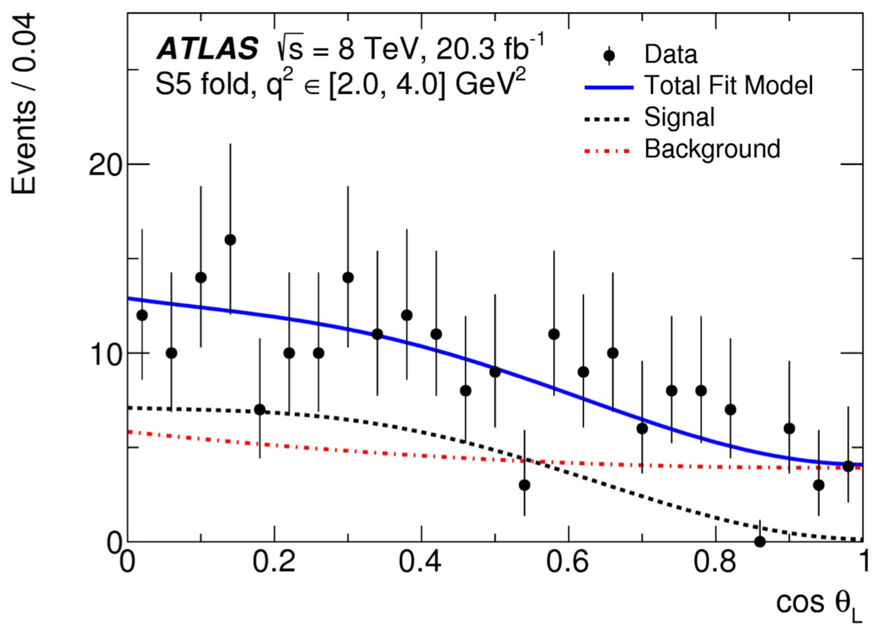

Results

- There is good agreement between theory and measurement for all regions with the exception of:
  - the P_4' and P_5' parameters in $q^2 \in [4.0, 6.0]$ GeV^2
  - P_8' parameter in $q^2 \in [2.0, 4.0]$ GeV^2